Water Research 88 (2016) 428–448

Contents lists available at ScienceDirect

Water Research

journal homepage: www.elsevier.com/locate/watres

Review

Recent developments of zinc oxide based photocatalyst in water treatment technology: A review

Kian Mun Lee [a, **], Chin Wei Lai [a], Koh Sing Ngai [c], Joon Ching Juan [a, b, *]

[a] Nanotechnology & Catalysis Research Centre (NANOCAT), 3rd Floor, Block A, Institute of Postgraduate Studies (IPS), University of Malaya, 50603 Kuala Lumpur, Malaysia
[b] School of Science, Monash University, Sunway Campus, Jalan Lagoon Selatan, Bandar Sunway 46150, Malaysia
[c] Department of Chemistry, Faculty of Science, Universiti Putra Malaysia, 43400 UPM Serdang, Selangor Darul Ehsan, Malaysia

ARTICLE INFO

Article history:
Received 22 July 2015
Received in revised form
28 September 2015
Accepted 28 September 2015
Available online 28 October 2015

Keywords:
Zinc oxide
Photocatalysis
Wastewater
Dopant
Pollutant

ABSTRACT

Today, a major issue about water pollution is the residual dyes from different sources (e.g., textile industries, paper and pulp industries, dye and dye intermediates industries, pharmaceutical industries, tannery and craft bleaching industries, etc.), and a wide variety of persistent organic pollutants have been introduced into our natural water resources or wastewater treatment systems. In fact, it is highly toxic and hazardous to the living organism; thus, the removal of these organic contaminants prior to discharge into the environment is essential. Varieties of techniques have been employed to degrade those organic contaminants and advanced heterogeneous photocatalysis involving zinc oxide (ZnO) photocatalyst appears to be one of the most promising technology. In recent years, ZnO photocatalyst have attracted much attention due to their extraordinary characteristics. The high efficiency of ZnO photocatalyst in heterogeneous photocatalysis reaction requires a suitable architecture that minimizes electron loss during excitation state and maximizes photon absorption. In order to further improve the immigration of photo-induced charge carriers during excitation state, considerable effort has to be exerted to further improve the heterogeneous photocatalysis under UV/visible/solar illumination. Lately, interesting and unique features of metal doping or binary oxide photocatalyst system have gained much attention and became favourite research matter among various groups of scientists. It was noted that the properties of this metal doping or binary oxide photocatalyst system primarily depend on the nature of the preparation method and the role of optimum dopants content incorporated into the ZnO photocatalyst. Therefore, this paper presents a critical review of recent achievements in the modification of ZnO photocatalyst for organic contaminants degradation.

Contents

* Corresponding author. Nanotechnology & Catalysis Research Centre (NANOCAT), 3rd Floor, Block A, Institute of Postgraduate Studies (IPS), University of Malaya, 50603 Kuala Lumpur, Malaysia.
** Corresponding author.
E-mail addresses: leekianmun@um.edu.my (K.M. Lee), jcjuan@um.edu.my (J.C. Juan).

http://dx.doi.org/10.1016/j.watres.2015.09.045
0043-1354/

1. Introduction

Today, solar energy, radiant light and heat from the sun, is the most abundant clean energy source available. Despite the fact that solar energy strikes our earth in an hour is relatively higher than energy consumed by humans for entire year (Lewis, 2007). Thus, extensive research studies and development of materials that can efficiently harvest solar irradiation and used it for green environmental pollution management are essential. In this manner, photocatalysis which utilizes our renewable solar energy to activate the chemical reactions via oxidation and reduction is a sustainable technology to provide solution for environmental issue (Kudo and Miseki, 2009). This photocatalysis system has attracted great interest from science community as the most promising way to solve the environmental problems, especially getting rid of residual dyes pollutants from wastewater stream. Photocatalysis involved a photochemical reaction at a metal oxide semiconductor's surface, which must be at least two reactions occurring simultaneously, the first reaction involving oxidation, from photo-induced positive holes, and the second reaction involving reduction, from photo-induced negative electrons (Fujishima et al., 2008). Several types of promising photocatalyst, such as titanium dioxide (TiO_2), zinc oxide (ZnO), iron(III) oxide (Fe_2O_3), zirconia (ZrO_2), vanadium(V) oxide (V_2O_5), niobium pentoxide (Nb_2O_5) and tungsten trioxide (WO_3) have been actively applied in environmental waste management system (Kudo and Miseki, 2009; Vinu and Madras, 2010).

In the field of photocatalysis today, ZnO has emerged as the leading candidate as an efficient and promising candidate in green environmental management system because of its unique

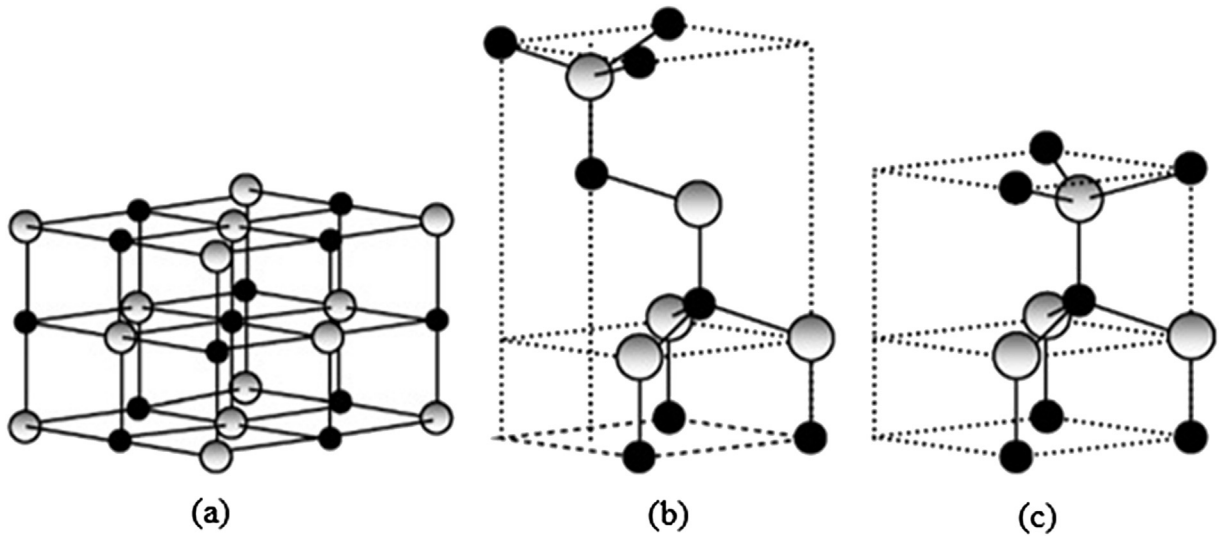

Fig. 1. The (a) rocksalt (cubic), (b) zinc blende (cubic) and (c) wurtzite (hexagonal) structures model of ZnO [23].

characteristics, such as direct and wide band gap in the near-UV spectral region, strong oxidation ability, good photocatalytic property, and a large free-exciton binding energy (Janotti and Van de Walle, 2009; Reynolds et al., 1999; Chen et al., 1998) so that excitonic emission processes can persist at or even above room temperature. It is a well-known fact that ZnO occurs as white hexagonal crystal or white powder known as zinc white. ZnO crystallizes in the wurtzite structure (Fig. 1), the same as GaN, but, in contrast, ZnO is available as large bulk single crystals (Reynolds et al., 1996). Besides, it is odourless, has a bitter taste and insoluble in water. As an important semiconductor material, ZnO has been applied in catalysis (King and Nix, 1996), rubber and paint industries, ceramic bodies, varistors, fertilizers and in cosmetics (Porter, 1991). However, an obvious hindrance to the widespread use of ZnO as a photoelectrode is ZnO exhibited lack of control over its electrical conductivity due to the n-type of ZnO crystals, which has been a matter of extensive debate and research (Janotti and Van de Walle, 2009; Ogale, 2005; Nickel and Terukov, 2005; Look, 2001). Thus, development of the ZnO with precisely controllable nanoscale features has gained significant scientific interest recently.

It will be seen in this review of the fundamentals and selected applications of photocatalysis, principally on ZnO and modified ZnO, that there is a host of possible photochemical, chemical and electrochemical reactions that can occur on the photocatalyst surface (Vinu and Madras, 2010). Clearly, with so many varied aspects, photocatalysis is nearly impossible to review comprehensively. In the present review, we have tried to summarize an overview of some of the more fundamental aspects, which are in their own right extremely scientifically interesting and which also need to be better understood in order to make significant progress and development with applications.

This review manuscript will be divided into several sections: 1. Introduction of ZnO; 2. Strategies to improve ZnO photodegradation efficiency; 3. Factors affecting photodegradation efficiency; 4. Advancement of ZnO in removing organic contaminants; 5. ZnO photocorrosion; 6. Conclusion and future work.

1.1. Properties of ZnO

ZnO is a wide band-gap semiconductor with large exciton binding energy of 60 meV at room temperature (Janotti and Van de Walle, 2009; Peng et al., 2006). The electrical, optical and magnetic properties of ZnO can be altered or improved by the use of ZnO in nanoscale (Shrama et al., 2014; Schmidt-Mende and MacManus-Driscoll, 2007). ZnO is an environmental friendly material as it is compatible with living organisms, which lending itself nicely to a broad range of daily applications that will not leave any risks to human health, and environmental impacts (Schmidt-Mende and MacManus-Driscoll, 2007). ZnO has received much attention in the degradation and complete mineralization of environmental pollutants (Anandan et al., 2010; Hasnat et al., 2007; Peternel et al., 2007). Since ZnO has almost the same band gap energy as TiO_2 (3.2 eV), its photocatalytic capability is anticipated to be similar to that of TiO_2. Moreover, ZnO is relatively cheaper compared to TiO_2 whereby the usage of TiO_2 are uneconomic for large scale water treatment operations (Daneshvar et al., 2004). The greatest advantage of ZnO is the ability to absorb a wide range of solar spectrum and more light quanta than some semiconducting metal oxides (Behnajady et al., 2006). The major drawbacks of ZnO are the wide band gap energy and photocorrosion. The light absorption of ZnO is limited in the visible light region which is due to its wide band energy. This results in fast recombination of photogenerated charges and thus caused low photocatalytic efficiency (Gomez-Solís et al., 2015).

Table 1
Optical and electrical properties of single crystal wurzite.

Property	Value
Energy band-gap (E_g)	3.2–3.7 eV (Direct)
Exciton binding energy	60 meV
Effective electron mass (M^*)	0.24–0.30 m_e
Effective hole mass (m_h^*)	0.45–0.60 m_e
Electron Hall mobility at 300 K for n-type (μ_e)	200 $cm^2\ V^{-1}\ S^{-1}$
Electron Hall mobility at 300 K for p-type	5–50 $cm^2\ V^{-1}\ S^{-1}$
Refractive index (nw, ne)	2.008, 2.029
Intrinsic carrier concentration (n)	$<10^6\ cm^{-3}$
Background carrier doping	n-type: $\approx 10^{20}$ electron cm^{-3} p-type: 10^{19} holes cm^{-3}
Optical transmission, T ($1/\alpha$)	80–95%

1.1.1. ZnO structure

ZnO has well-defined crystal structures which are commonly in rocksalt, wurtzite or cubic (zinc blende) structure. A rocksalt structure of ZnO can be yielded under high pressure thus ZnO in this structure is quite rare. The ZnO wurtzite structure has the highest thermodynamic stability among the three structures. It is the most common structure of ZnO (Dubbaka, 2008; Özgür et al., 2005 and Wang, 2004). ZnO has a hexagonal wurtzite crystal structure at ambient pressure and temperature, with two lattice parameters, *a* and *c*, values of 0.3296 nm and 0.52065 nm, respectively (Dubbaka, 2008; Baruah and Dutta, 2009). This ZnO hexagonal wurtzite space grote structure belongs to the P63mc space group and exhibits a non-centrosymmetric structure, which causes ZnO to be piezoelectric and pyroelectric (Moore and Wang, 2006). Non-centrosymmetric structure of ZnO is the condition at where the space groups lack inversion centre (Maggard et al., 2001). Fig. 1 exhibits the unit cell of rocksalt, zinc blende and wurtzite structures of ZnO (Morkoç and Özgür, 2009).

It could be observed that the wurtzite ZnO consists of atoms forming hexagonal-close-pack sub-lattices which will stack alternatively along the *c*-axis (Erhart and Albe, 2006). In this case, each Zn^{2+} sub-lattice contains four Zn^{2+} ions and surrounded by four O^{2-} ions and vice versa, coordinated at the edges of a tetrahedron (Jagadish and Pearton, 2006). This tetrahedral coordination will form polar symmetry along the hexagonal axis which induces the effect of piezoelectricity and spontaneous polarization in the ZnO wurtzite crystal (Kong and Wang, 2003; Hughes and Wang, 2004). The polarization effect is one of the major factors influencing the crystal growth during the synthesis process of ZnO nanostructures (Wang, 2004). Fig. 1 presents the shaded grey and black spheres denote Zn and O atoms, respectively.

1.1.2. Mechanical properties of ZnO

Typically ZnO has a relatively low hardness ranged from 4 to 5 GPa at different indentations (Fang et al., 2007; Kucheyev et al.,

Table 2
Phonon modes of wurtzite ZnO at room temperature.

Phonon mode	Value (cm^{-1}): single crystal
E_2^{low}	101
E_2^{high}	437
TO (A1)	380
LO (A1)	574
TO (E1)	591

2002). This value has to be taken into consideration during the processing and designing of ZnO devices. Indentation to the ZnO structure will result in significant quenching of excitonic luminescence (Zhang et al., 2014c). The crystal orientation of ZnO as seen previously also results in different mechanical properties. The *a*-axis oriented bulk ZnO has lower hardness which is 2 GPa compared to *c*-axis oriented ZnO (Zhang et al., 2014c; Jian et al., 2008). From the aspect of epitaxial ZnO, studies have shown that the epitaxial ZnO grown on sapphire has higher hardness than the bulk ZnO (Hwang et al., 2007). The hardness is 5.75 GPa for *c*-axis epitaxial layers (Coleman et al., 2005).

1.1.3. Electrical and optical properties of ZnO

ZnO has a direct band-gap of 3.37 eV and a large exciton binding energy of 60 meV at room temperature with good electro-optical properties and high electrochemical stability (Lu et al., 2006; Tan et al., 2005). The ZnO is very stable chemically, thermally and also under high energy radiation (Lu et al., 2006; Tan et al., 2005; Liu et al., 2010; Rodnyi and Khodyuk, 2011). The n-type ZnO semiconductor has wide direct band gap, higher electron mobility, high breakdown voltages, and higher breakdown field strength (Liu et al., 2010; Rodnyi and Khodyuk, 2011; Umar, 2009). The optical and electrical properties of single crystal wurzite are presented in Table 1. In this manner, ZnO has been used specifically in high powered electronic devices such as for field emission devices due to its excellent electrical devices. In addition, modified ZnO has also been used for transparent conducting electrode for several types of optoelectronic devices. The recombination of generated electron and hole pairs in ZnO would produce UV/blue light (Rodnyi and Khodyuk, 2011; Umar, 2009). Thus, ZnO has been used for short wavelength optoelectronics such as UV/blue light emitter applications (Lu et al., 2006). Table 1 shows the optical and electrical properties of single crystal wurzite. (Adapted and modified from Jagadish and Pearton, 2006).

1.1.4. Luminescence and lattice dynamics properties of ZnO

The luminescence properties of ZnO can be characterized using photoluminescence (PL). Typical PL spectra exhibited by ZnO nanostructure consist of two regions, which are the UV-emission region and broad visible emission (Wang et al., 2007; Hong et al., 2008b). In this case, UV emission which is also termed as deep level emission is attributed to the recombination of excitons (electron–hole pair recombination or band to band recombination) (Hullavarad et al., 2009; Sharmaa et al., 2010). If the ZnO is highly crystalline, then the UV emission would be very high (Hullavarad et al., 2009). The origin of the green band in the visible region in ZnO is attributed to various impurities and defects (Morkoç and Özgür, 2009). The visible emission could be related to the recombination of electrons with oxygen vacancies and with photoexcited holes in the valence band and hence its increase in intensity maybe attributed to the large defect concentration (Kurbanov et al., 2011).

Lattice dynamics of a single crystal wurtzite ZnO can be measured by using Raman spectroscopy analysis. In a perfect wurtzite ZnO crystal, the 4 atoms per unit cell will correspond to 12 phonon modes. The modes are one longitudinal-acoustic (LA), two transverse-acoustic (TA), three longitudinal-optical (LO) and six transverse-optical (TO) branches. Table 2 presents the most common Raman modes depicted by various authors on the value obtained from single crystal wurtzite ZnO at room temperature (Jagadish and Pearton, 2006).

1.1.5. ZnO thermal properties

Thermal properties of ZnO include thermal expansion coefficient, thermal conductivity and specific heat (Jagadish and Pearton, 2006). Thermal expansion coefficient of a material is the lattice deformation as a function of temperature. ZnO has thermal expansion coefficients at the *a*-axis of $\alpha = 4.31 \times 10^{-6}\ K^{-1}$ and *c*-axis of $\alpha = 2.49 \times 10^{-6}\ K^{-1}$ at 300 K (Morkoç and Özgür, 2009). Thermal conductivity is defined as the ability of a material to conduct heat. It is vital especially when the devices are to be used under high power and high temperature conditions. Factors that influence the thermal conductivity in a ZnO semiconductor material too as ZnO semiconductor contains a large number of point defects, which make the effect significantly felt as in other semiconductors. The typical thermal conductivity values are in the range from 0.6 W $cm^{-1}\ K^{-1}$ to 1 W $cm^{-1}\ K^{-1}$. Specific heat is the heat capacity per unit mass of material. In fact, the specific heat of a material is influenced by the lattice vibrations, free carriers and number of defects presence within a material. The specific heat capacity of ZnO at constant pressure is measured as $C_p = 40.3\ J\ mol^{-1}\ K^{-1}$ (Sun et al., 2006).

1.2. Fundamental and photocatalytic degradation mechanism of ZnO

1.2.1. Photocatalysis

The term photocatalysis consists of the combination of photochemistry and catalysis (Serpone and Pelizzetti, 1989). It implies that light and a catalyst are necessary to bring about or to accelerate a chemical transformation. In other words, photocatalysis can be defined as "acceleration of a photoreaction in the presence of a catalyst". This definition includes photosensitization, *i.e.* a process by which a photochemical alteration occurs in one chemical species as a result of initial absorption of radiation by another chemical species called the photosensitizer.

It follows from the above that heterogeneous photocatalysis involves photoreactions which occur at the surface of a catalyst. If the adsorbate is photoexcited first and then interacts with the ground state of the catalyst substrate, the process is referred to sensitized photoreaction. On the other hand, if the catalyst is photoexcited first and then interacts with the ground state adsorbate molecule, the process is a "catalyzed photoreaction". In most cases, heterogeneous photocatalysis refers to semiconductor photocatalysis or semiconductor-sensitized photoreactions (Mills and Hunte, 1997).

1.2.2. Semiconductor photocatalysis mechanism

In an ideal photocatalytic process, organic pollutants are mineralized into carbon dioxide (CO_2), water (H_2O) and mineral

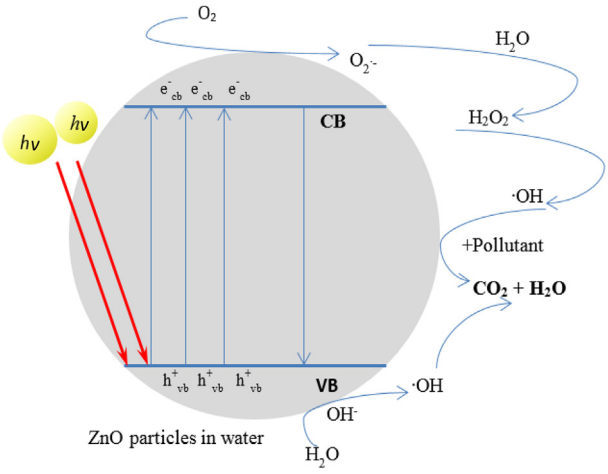

Fig. 2. General mechanism of the photocatalysis [47].

Table 3
Influence of an anionic dopant on photocatalytic activity of ZnO.

Dopant	Light source/pollutant	Experimental conditions	Photodegradation efficiency (%)		Reference
			ZnO	Doped ZnO	
C	Sunlight (Intensity = 1.08×10^5 lux) Rhodamine B (RhB)	Catalyst = 1 g/L [RhB] = 4.8 mg/L Irradiation time: 30 min	40.0	100	Haibo et al., 2014
C	Solar simulator (Intensity = 80 lux) Methylene Blue (MB)	Catalyst = 0.4 g/L [MB] = 3.2 mg/L Irradiation time: 210 min	13.9	42.3	Samadi et al., 2013
N	1000 W Xe lamp Rhodamine 6G (R6G)	Catalyst = 0.1 g/L [R6G] = 500 mg/L Irradiation time: 80 min	5.4	81.6	Wu et al., 2013
N	350 W Xe lamp Bisphenol A (BPA)	Catalyst = 0.33 g/L [BPA] = L/L Irradiation time: 4 h	~25.0	93.0	Qiu et al., 2013
N	350 W Xe lamp Methyl Orange (MO)	Catalyst = 0.4 g/L [MO] = 10 mg/L Irradiation time: 100 min	20.0	100	Sun et al., 2013
S	Sunlight Resorcinol (Rs)	Catalyst = 2.5 g/L [Rs] = 150 mg/L Irradiation time: 420 min	~55.0	100	Patil et al., 2010

acids in the presence of ZnO particle and reactive oxidizing species, such as oxygen or air. The photocatalytic reactions were initiated when ZnO particle absorbs photons with energies greater than that of its band gap energy from the illumination. In this way, photo-induced electron is promoted from the valence band (VB) to the conduction band (CB), forming positively hole (h^+_{VB}) and electron (e^-_{CB}) on the surface of ZnO particle (Eq. (1)).

$$ZnO + h\nu \rightarrow ZnO\left(e^-_{CB} + h^+_{VB}\right) \quad (1)$$

$$e^-_{CB} + h^+_{VB} \rightarrow heat \quad (2)$$

$$e^-_{CB} + O_2 \rightarrow \cdot O_2^- \quad (3)$$

$$h^+_{VB} + OH^- \rightarrow \cdot OH \quad (4)$$

$$\cdot OH + R - H \rightarrow R^{'\cdot} + H_2O \quad (5)$$

$$h^+_{VB} + R \rightarrow R^{+\cdot} \rightarrow Intermediates \quad (6)$$

$$e^-_{CB} + O_2 \rightarrow \cdot O_2^- + H^+ \rightarrow HOO\cdot + \cdot O_2^- \rightarrow HOO\cdot + O^- \quad (7)$$

$$HOO\cdot \rightarrow H_2O_2 + O_2 \quad (8)$$

$$H_2O_2 + \cdot O_2^- \rightarrow \cdot OH + OH^- + O_2 \quad (9)$$

It should be noted the photo-generated holes in the valence band will recombine with the photo-excited electrons in the conduction band and dissipates in the form of heat (Eq. (2)). Therefore, the presence of oxygen as electron scavengers prolong the recombination of electron–hole pair while forming the superoxide radicals ($\cdot O_2^-$) (Eq. (3)). The reaction of h^+_{VB} with OH^- (Eq. (4)) may leads to the formation of hydroxyl radicals. The hydroxyl radical is an extremely strong, non-selective oxidant ($E^0 = +3.06$ V) which leads to the partial or complete mineralization of organics (Eq. (5)). Moreover, the high oxidative potential of the hole in the photocatalyst also permits the direct oxidation of organic matter to reactive intermediates as shown in Eq. (6). The superoxide radicals was further protonated to produce hydroperoxyl radical (HOO•) and subsequently H_2O_2 (Eqs. (7)–(9)). The HOO• also functions as electron scavengers to trap conduction band electrons which further delay the recombination process. The general photocatalysis mechanism processes are shown in Fig. 2.

2. Strategies to improve ZnO photodegradation efficiency

The recombination of photogenerated hole (h^+_{VB}) and electron (e^-_{CB}) is the major disadvantage in semiconductor photocatalysis. This recombination step lowers the quantum yield and causes energy wasting. Therefore, the e^-–h^+ recombination process should be inhibited to ensure efficient photocatalysis. Metal doping could counter the recombination problem by enhancing the charge separation between electrons and holes. In addition, the dopants may trap electrons, reducing the chances of electron–hole recombination that deactivates the photocatalytic system (Sanchez and Lopez, 1995). Furthermore, the generation of hydroxyl radicals and active oxygen species will greatly increase resulted from enhancement in charge separation efficiency (Kato et al., 2005). Generally, the concentration and ion nature of the dopant, synthesis method and operating conditions significantly affect the photoactivity of the metal-doped semiconductor. The introduction of different types of metal dopant into a semiconductor, namely anionic dopant, cationic dopant and rare-earth dopant will be discuss in the

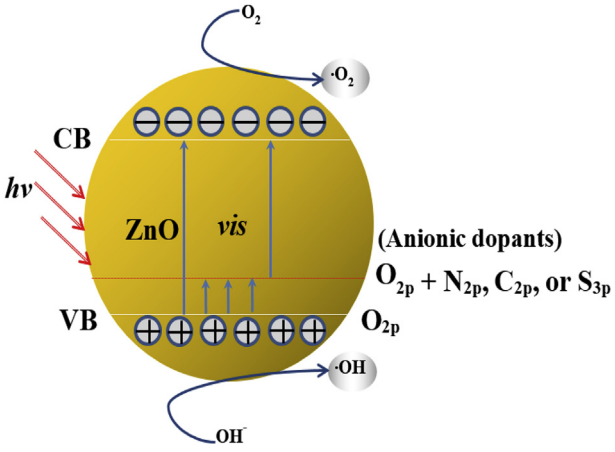

Fig. 3. Photocatalytic mechanism by an anionic dopant on ZnO surface.

following sections.

2.1. Anionic dopants

As tabulated in Table 3, an anionic-doped ZnO photocatalyst exhibited enhanced photocatalytic degradation performance compared to that of pure ZnO. In the case of N–ZnO system, the existence of isolated N 2p states above the valence band maximum of ZnO increased its visible light absorption ability. Hence, the photogenerated electron–hole pairs exist between the impurity N 2p states and Zn 3d conduction band. Additionally, the narrowing band gap in N–ZnO system requires less energy to photoinduce the charge carriers, i.e. electron and hole, under visible light irradiation (Batzill et al., 2006; Irie et al., 2003). In such a way, the photoexcited e^-_{CB} could be reacted with surface adsorbed oxygen to produce superoxide radical anions which subsequently converted to hydroxyl radicals (Nagaveni et al., 2004; Dong et al., 2009; Chu et al., 2012). Meanwhile, the h^+_{VB} will react with the adsorbed hydroxyl anion to form hydroxyl radicals. These $O_2^{\cdot-}$ and •OH were used in the photodegradation of organic contaminants. The reaction mechanism is summarized as below:

$$ZnO - N \rightarrow h^+_{VB} + e^-_{CB} \quad (10)$$

$$O^{\cdot-}_{2\,ads} + H_2O \rightarrow \cdot OH + OH^- \quad (11)$$

$$H_2O \rightarrow OH^-_{ads} + H^+ \quad (12)$$

$$OH^-_{ads} + h^+_{VB} \rightarrow \cdot OH \quad (13)$$

$$\cdot OH + \text{organic contaminant} \rightarrow \text{degradation products} + CO_2 + H_2O \quad (14)$$

Guo et al. (2009) reported that the increment in photocatalytic activity of carbon-doped ZnO could attributed to several reasons. First, the presence of carbon on C–ZnO surface enhanced the MB adsorption on the catalyst surface. Second, C–ZnO showed stronger UV absorption in comparison to the pure ZnO. Third, the surface oxygen vacancies in the ZnO nanostructure induced new energy levels below the conduction band of ZnO, where the photo-excited electrons were scavenged by this new energy levels and the recombination of electron–hole is avoided. These increased the number of charge carriers, which improved the photodegradation efficiency (Lai et al., 2011; Li et al., 2012b, 2009; Wang et al., 2009a; Maiti et al., 2012; Liu et al., 2009; Zheng et al., 2007).

Similarly, the number of oxygen vacancies play a significant role in affecting the photoactivity of S-doped ZnO system. During the photocatalytic process, the oxygen vacancies and defects become centers to trap photogenerated electrons. As a result, the electron–hole recombination process is hindered. Therefore, the higher the amount of oxygen vacancy or defect, the better the photocatalytic activity (Patil et al., 2010). Chen et al. (2008) synthesized N,S,C–ZnO by precipitation route and found that the interfering of the non-metal dopants with ZnO crystallization improved the photoactivity by enhancement in light absorption and more efficient in transportation of electron–hole. Fig. 3 illustrates the schematic diagram on the photocatalytic mechanism by an anionic dopant on ZnO surface.

2.2. Cationic dopants

Some properties of ZnO is important for its practical applications in various fields. Preparation of new photocatalyst by incorporation of other elements is an important challenge in the development of ZnO photocatalyst. Although ZnO is a good photocatalyst, the doped ZnO surpasses its photocatalytic efficiency. Modification of ZnO by cationic dopants is currently another important technology being used by many researchers. The doped ZnO possesses prominent photodegradation performance than the undoped ZnO. Moreover, the structural, optical, chemical, electrical and magnetic properties of ZnO can be tuned by the addition of selected cationic dopant. The ZnO have been doped with elements such as Al, Sb, Mn, Ni, Co have enhanced photocatalytic performance. The cationic doping is performed essentially by the addition of transition metals, group I and group V elements. The incorporated elements are usually isomorphic to zinc ions, such as Cu^{2+}, Ni^{2+}, Co^{2+} and Mn^{2+}. The effective of a new photocatalyst can be characterized by photodegradation of a selected organic pollutant. In recent years, many photocatalytic studies reveal that the cationic dopant strongly improved the photocatalytic activity of ZnO. The results indicated that the cationic doped ZnO have better photocatalytic activity than the undoped ZnO. The doped ZnO exhibits faster response to the photodegradation of many organic pollutants. The influence of various cationic dopants in the photocatalyitc property of ZnO is summarized in Table 4. Comparison of the photodegradation in various organic pollutants is studied on both undoped and cationic doped ZnO.

The photocatalytic properties of the Se-doped ZnO were compared with the undoped ZnO. The Se-doped ZnO showed the higher photodegradation activity towards Trypan Blue (Dutta et al., 2014; Nenavathu et al., 2013). Methylene Blue is commonly used as model organic pollutant for the photocatalytic study. A number of transition metals including Cd (Zhang and Zeng, 2012), Fe (Kumar et al., 2014a), Hf (Ahmad et al., 2013c) and Pd (Han et al., 2013), have been used as dopants. It can be seen from Table 4 that 1.0 M% Fe-doped ZnO shows the highest photocatalytic activity among all modified ZnO catalysts towards the degradation process of Methylene Blue. Among all cationic modified ZnO, transition elements modified ZnOs have wide popularity in the photodegradation of Methyl Orange (Karunakaran et al., 2011; Zhong et al., 2012b; Saleh and Djaja, 2014; Ahmad et al., 2013a; Wu et al., 2012). Enhanced photocatalytic removal of Methyl Orange upon doping the ZnO with Al was previously observed (Xiaoliang et al., 2013; Zhang et al., 2014b; Ahmad et al., 2013b). Although many modified ZnO showed enhanced photocatalytic activity, in some cases, the doping does not significantly influence the photocatalytic activity. For example, photodegradation of phenol by 10 M% Li-loaded ZnO (Benhebal et al., 2012) and photocatalytic removal of Methyl Orange by 0.9 at. % Ag-loaded ZnO (Karunakaran et al., 2011) and 15 at. % Na-loaded ZnO (Xiaoliang et al., 2013).

The photocatalytic activities of some alkali metal-doped ZnO have been evaluated using phenol and organic dye pollutants. Enhanced performance was observed with Na-doped ZnO over undoped ZnO in the photodegradation of Methyl Orange (Xiaoliang et al., 2013) and Methylene Blue (Kim et al., 2013), respectively. Low doping level of K-doped ZnO exhibits satisfied photocatalytic performance when employed for photodegradation of Rhodamine B (Li et al., 2014b), whereas high doping level of K-doped ZnO showed reduced in the photocatalytic activity over the undoped ZnO (Benhebal et al., 2012). The results suggested that the photodegradation efficiency of K-doped ZnO is more prominent by loading an appropriate amount of K.

The photocatalytic reaction begins with the generation of electrons and holes under irradiation. These photogenerated charges are moved to the catalyst surfaces separately. Electrons react with oxygen molecules to form superoxide anions. Both electrons and holes react in the solution lead to the formation of highly oxidizing species such as hydroxyl and hydroperoxyl radicals. These radicals are responsible in the photooxidation of organic pollutants. The mechanism for photocatalytic degradation of the organic pollutants is proposed as below:

Table 4
Influence of a cationic dopant on photocatalytic activity of ZnO.

Dopant	Light source/pollutant	Experimental conditions	Photodegradation efficiency (%)		Reference
			ZnO	Doped ZnO	
Ag (6.7 mol%)	8 W UV lamp 17 α-ethinylestradiol (EE2)	Catalyst = 0.5 g/L [EE2] = 2.7 mg/L Irradiation time = 50 min	53.0	~100	Li et al., 2014c
Ag (0.9 at.%)	Hg lamp Methyl Orange (MO)	Catalyst = 0.8 g/L [MO] = 50 mg/L Irradiation time = 40 min	20.0	30.0	Karunakaran et al., 2011
Ag (0.5 M%)	UV lamp 4-Nitrophenol (4-NP)	Catalyst = 2 g/L [4-NP] = 10 mg/L Irradiation time = 180 min	~15.0	100	Divband et al., 2013
Al (10 at.%)	2 × 20 W UV lamp Methyl Orange (MO)	Catalyst = 0.5 g/L [MO] = 10 mg/L Irradiation time = 180 min	50.0	95.7	Xiaoliang et al., 2013
Al (1.5 mol%)	500 W halogen lamp Methyl Orange (MO)	Catalyst = 0.6 g/L [MO] = 3.3 mg/L Irradiation time = 150 min	20.2	95.9	Zhang et al., 2014b
Al (4.0 M%)	400 W halogen lamp Methyl Orange (MO)	Catalyst = 1 g/L [MO] = 10 mg/L Irradiation time = 150 min	13.0	20.0	Ahmad et al., 2013b
Bi (5.0 at.%)	UV lamp Congo Red (CR)	Catalyst = 1.67 g/L [CR] = 69.7 mg/L Irradiation time = 60 min	80.0	~86.0	Chandraboss et al., 2013
Bi (5.0 M%)	300 W Hg lamp Methyl Orange (MO)	Catalyst = 1 g/L [MO] = 10 mg/L Irradiation time = 60 min	26.0	46.2	Zhong et al., 2012b
Cd (5 at.%)	9 W UV lamp Rhodamine B (RhB)	Catalyst = 0.9 g/L [RhB] = 24 mg/L Irradiation time = 180 min	70.0	98.0	Zhai et al., 2014
Cd (1.2 at.%)	500 W Halogen lamp Methylene Blue (MB)	Catalyst = 0.025 g/L [MB] = 10 mg/L Irradiation time = 200 min	10.0	55.0	Zhang and Zeng, 2012
Co (12.0 at.%)	2 × 20 W UV lamp Methyl Orange (MO)	Catalyst = 0.2 g/L [MO] = L/L Irradiation time = 120 min	~60.0	~70.0	Saleh and Djaja, 2014
Co (0.25 at.%)	150 W Xe lamp Rhodamine B (RhB)	Catalyst = 0.16 g/L [RhB] = 9.6 mg/L Irradiation time = 90 min	~100	~90.0	He et al., 2012
Cu (3.0 wt.%)	400 W halogen lamp Methyl Orange (MO)	Catalyst = 1 g/L [MO] = L/L Irradiation time = 120 min	26.0	39.0	Ahmad et al., 2013a
Cu (15 wt.%)	350 W UV lamp Resazurin (Rz)	Catalyst = 0.1 g/L [Rz] = 1.5 mg/L Irradiation time = 25 min	60.0	90.0	Mohan et al., 2012
Cu (3.0 mol%)	1000 W Xe lamp Methyl Orange (MO)	Catalyst = 0.01 g/L [MO] = 9.8 mg/L Irradiation time = 140 min	5.1	~40.0	Wu et al., 2012
Fe (1.0 M%)	2 × 18 W UV lamps Methylene Blue (MB) [MB] = 32 mg/L Irradiation time = 105 min	Catalyst = 0.45 g/L	5.0	42.0	Kumar et al., 2014a
Fe (1.0 M%)	500 W Xe lamp Rhodamine B (RhB)	Catalyst = 1 g/L [RhB] = 10 mg/L Irradiation time = 90 min	67.0	94.0	Yi et al., 2014
Fe (0.5 wt.%)	Sunlight (Intensity = 23 W/m^2) 2-Chlorophenol (2-CP)	Catalyst = 1 g/L [2-CP] = 50 mg/L Irradiation time = 90 min	~65	~85	Ba-Abbad et al., 2013
Hf (2 mol%)	Sunlight (1.263 × 10^5 lux) Methylene Blue (MB)	Catalyst = 0.25 g/L [MB] = 250 mg/L Irradiation time = 90 min	50.0	85.0	Ahmad et al., 2013c
K (0.3%)	500 W Xe lamp Rhodamine B (RhB)	Catalyst = 0.5 g/L [RhB] = 4.8 mg/L Irradiation time = 80 min	42.1	92.6	Li et al., 2014b
K (10%)	125 W UV lamp Phenol (Ph)	Catalyst = 1 g/L [Ph] = 200 mg/L Irradiation time = 120 min	~70.0	~60.0	Benhebal et al., 2012
Li (10%)	125 W UV lamp Phenol (Ph)	Catalyst = 1 g/L [Ph] = 200 mg/L Irradiation time = 120 min	~70.0	~75.0	Benhebal et al., 2012
Li (10 wt.%)	1000 W Xe lamp Methylene Blue (MB)	Catalyst = 1.2 g/L [MB] = 3.2 mg/L Irradiation time = 40 min	53.1	100	Ganesh et al., 2012
Mg (5 wt.%)	125 W Hg lamp Alprazolam (APZ)	Catalyst = 1 g/L [APZ] = 9.3 mg/L Irradiation time = 5 min	~60.0	~80.0	Ivetić et al., 2014

Table 4 (*continued*)

Dopant	Light source/pollutant	Experimental conditions	Photodegradation efficiency (%)		Reference
			ZnO	Doped ZnO	
Mg (5%)	3 × 18 W Blacklight blue lamp Methylene Blue (MB)	Catalyst = 1 g/L [MB] = 3.2 mg/L Irradiation time = 60 min	83.0	92.0	Suwanboon et al., 2013
Mg (10%)	Simulated sunlight Intensity = 0.68 W/m^2 Methylene Blue (MB)	Catalyst = 1.2 g/L [MB] = 3.2 mg/L Irradiation time = 9 min	~83.3	100	Etacheri et al., 2012
Mn (12.0 at.%)	2 × 20 W UV lamp Methyl Orange (MO)	Catalyst = 0.2 g/L [MO] = L/L Irradiation time = 120 min	~60.0	~85.0	Saleh and Djaja, 2014
Mn (1%)	6 W UV lamp *o*-cresol	Catalyst = 1.5 g/L [*o*-cresol] = 35 mg/L Irradiation time = 360 min	79.0	88.0	Abdollahi et al., 2011
Na (15 at.%)	2 × 20 W UV lamp Methyl Orange (MO)	Catalyst = 0.5 g/L [MO] = 10 mg/L Irradiation time = 180 min	50.0	55.5	Xiaoliang et al., 2013
Na (1.86 wt.%)	500 W Xe lamp Methylene Blue (MB)	Catalyst = 1 g/L [MO] = 10 mg/L Irradiation time = 180 min	~31.8	100	Kim et al., 2013
Pd (1.5 at.%)	UV lamp Methylene Blue (MB)	Catalyst = 0.1 g/L [MB] = 9.6 mg/L Irradiation time = 30 min	68.0	~100	Han et al., 2013
Pd (3 M%)	300 W Hg lamp Methyl Orange (MO)	Catalyst = 1 g/L [MO] = 10 mg/L Irradiation time = 60 min	30.0	~50.0	Zhong et al., 2012a
Sb (3 mol%)	UV lamp Methylene Blue (MB)	Catalyst = 1 g/L [MB] = 3.2 mg/L Irradiation time = 300 min	56.0	95.0	Phuruangrat et al., 2014a
Sb (0.03 mol%)	125 W UV lamp Methylene Blue (MB)	Catalyst = 0.4 g/L [MB] = 8.8 mg/L Irradiation time = 40 min	71.9	~100	Omidi et al., 2013
Se (5 wt.%)	25 W UV lamp Trypan Blue (TrB)	Catalyst = 0.6 g/L [TrB] = 17.5 mg/L Irradiation time = 360 min	18.0	85.0	Dutta et al., 2014
Se (5 wt.%)	30 W UV lamp Trypan Blue (TrB)	Catalyst = 0.6 g/L [TrB] = 17.5 mg/L Irradiation time = 360 min	16.5	86.1	Nenavathu et al., 2013
Sn (1 M%)	300 W Hg lamp Methyl Orange (MO)	Catalyst = 1 g/L [MO] = 10 mg/L Irradiation time = 60 min	26.0	68.0	Li et al., 2013
Sr (0.1 M%)	1000 W Xe lamp Rhodamine B (RhB)	Catalyst = 1 g/L [RhB] = 10 mg/L Irradiation time = 180 min	30.0	92.0	Li et al., 2014a

$$ZnO + h\nu \rightarrow ZnO\left(e^-_{CB} + h^+_{VB}\right) \quad (15)$$

$$e^-_{CB} + M^{n+} \rightarrow M^{(n-1)+} \quad (16)$$

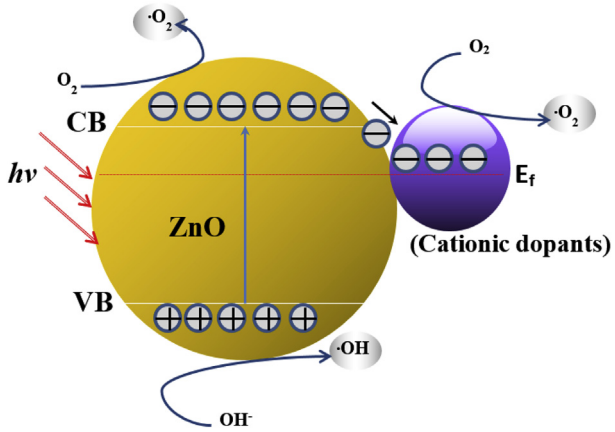

Fig. 4. Proposed photocatalytic degradation mechanism by a cationic dopant on ZnO surface.

$$O_2 + M^{(n-1)+} \rightarrow \cdot O_2^- + M^{n+} \quad (17)$$

$$ZnO\left(h^+_{VB}\right) + OH^- \rightarrow ZnO + \cdot OH \quad (18)$$

$$\cdot OH + \text{organic contaminant} \rightarrow \text{degradation products} + CO_2 + H_2O \quad (19)$$

When cationic dopant is added to ZnO, the photodegradation efficiency of ZnO is improved further. Several locations are possible for the cationic dopant deposition: the surface of the ZnO, the Zn sites within the lattice of ZnO crystal, and the interstitial sites of the ZnO in crystal lattice (He et al., 2012). Dopant also affects the interfacial electron transfer rate and recombination rate of the charge carriers. The incorporated elements such as K, Ni, Cu, Pd and Cd, could increase the specific surface area of ZnO and reduced the resistivity of ZnO. The presence of the dopants could also reduce the activation energy in the photocatalytic activity. The effective route leads to the high catalytic efficiency in the new photocatalyst. Cation-doped ZnO has a lower band gap energy value, compared to the undoped ZnO. When cationic dopants were introduced as impurities in the ZnO crystal lattice, extra energy levels are added to

Table 5
Influence of a rare earth dopant on photocatalytic activity of ZnO.

Dopant	Light source/pollutant	Experimental conditions	Photodegradation efficiency (%)		Reference
			ZnO	Doped ZnO	
Ce (2 at.%)	55 W compact fluorescence lamp Phenol	Catalyst = 1 g/L [Phenol] = L/L Irradiation time: 300 min	~60.0	~78.0	Sin et al., 2014a
Dy (3 mol%)	UV lamp Methylene Blue (MB)	Catalyst = 5 g/L [MB] = 3.2 mg/L Irradiation time: 300 min	56.0	98.0	Yayapao et al., 2013b
Er (4.8 M%)	32 W UV lamp Methylene Blue (MB)	Catalyst = 0.5 g/L [MB] = 10 mg/L Irradiation time: 60 min	69.3	97.7	Yu et al., 2013
Eu (1 mol%)	100 W Hg lamp Methyl Orange (MO)	Catalyst = 1 g/L [MO] = 10 mg/L Irradiation time: 180 min	75.7	95.3	Zong et al., 2014
Eu (3 mol%)	UV lamp Methylene Blue (MB)	Catalyst = 1.5 g/L [MB] = 3.2 mg/L Irradiation time: 300 min	75.0	90.5	Phuruangrat et al., 2014b
Eu (2 at.%)	55 W compact fluorescence lamp Phenol	Catalyst = 1 g/L [Phenol] = L/L Irradiation time: 300 min	~60.0	~86.0	Sin et al., 2014b
Gd (0.05 mol%)	125 W Hg lamp Rhodamine B (RhB)	Catalyst = 0.3 g/L [RhB] = 2.4 mg/L Irradiation time: 60 min	70.0	100.0	Kumar and Sahare, 2014b
Ho (3 mol%)	UV lamp Methylene Blue (MB)	Catalyst = 1.5 g/L [MB] = 3.2 mg/L Irradiation time: 300 min	74.8	98.3	Phuruangrat et al., 2014c
Nd (0.04 mol%)	125 W Hg lamp Rhodamine B (RhB)	Catalyst = 0.3 g/L [RhB] = 2.4 mg/L Irradiation time: 60 min	~70.0	100.0	Kumar and Sahare, 2012
Nd (1 mol%)	UV lamp Methylene Blue (MB)	Catalyst = 5 g/L [MB] = 3.2 mg/L Irradiation time: 300 min	55.0	92.0	Yayapao et al., 2013a
Nd (3 mol%)	UV lamp Methyl Orange (MO)	Catalyst = 1 g/L [MO] = 15 mg/L Irradiation time: 45 min	85.0	100.0	Zhao et al., 2014
Sm (1 at.%)	55 W compact fluorescence lamp 2,4-dichlorophenol (2,4-DCP)	Catalyst = 1 g/L [2,4-DCP] = L/L Irradiation time: 180 min	72.2	98.5	Sin et al., 2013

the new photocatalyst. The excitation of electrons are effective even with lower energy photons. Moreover, the incorporated elements act as electron traps, which suppress the recombination of photogenerated holes and electrons. Thus retarding the rate of electron–hole pairs formation. The dopants can extend the light absorption range and enhanced the photoresponse of the cation-loaded ZnO in visible light range. The overall photocatalytic activity is improved under the entire spectrum of sunlight.

However, high-doping level ZnO could reduce the photodegradation efficiency. This could be attributed to the physical defects and the increased oxidation states of cations. The excess cations may act as trapping sites for the holes and electrons, and thus promote the recombination of photogenerated charges. This progressively retards the generation of •OH and $\cdot O_2^-$ free radicals which leads to the reduction in photocatalytic activity. The schematic of the photocatalytic degradation of a cationic dopant on the surface of ZnO is shown in Fig. 4.

2.3. Rare earth dopants

Rare earth (RE) metal, another elegant dopant for the photodegradation of organic pollutants. Recently, rare earth doped photocatalyst have received much attention. The unique photocatalytic and redox properties of RE is important to promote the surface properties and the electron transfer activity of the photocatalyst. The RE-doped ZnO have been reported to exhibit better photocatalytic activity compared to the undoped ZnO. Table 5 summarized the literature of photocatalytic efficiency studies at undoped and RE-doped ZnOs. The Nd-loaded ZnO are considered to be a popular photocatalyst for the photodegradation study of various organic dyes such as Rhodamine B (Kumar and Sahare,

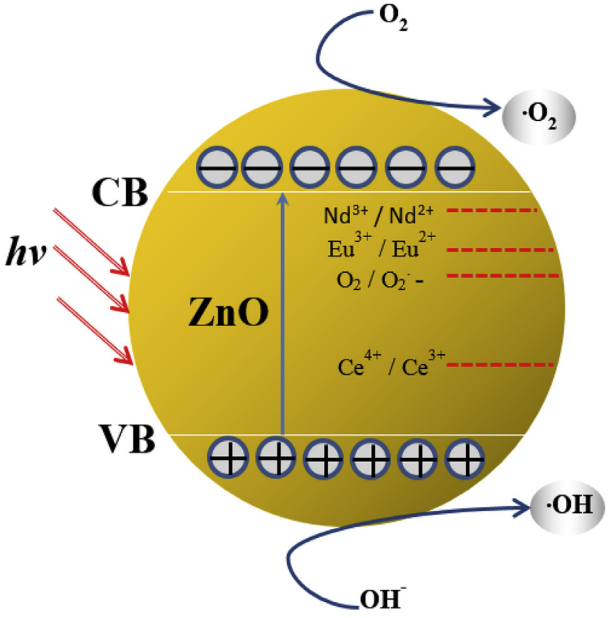

Fig. 5. The photodegradation of organic contaminants by a rare-Earth-ZnO photocatalyst.

Table 6
Influence of co-dopant on photocatalytic activity of ZnO.

Co-dopants M_1–M_2-ZnO	Light source/pollutant	Experimental conditions	Photodegradation efficiency (%)				Reference
			ZnO	M_1-ZnO	M_2-ZnO	M_1–M_2-ZnO	
Ag–Au–ZnO	4 × 8 W medium pressure Hg lamp Methylene Blue (MB)	Catalyst = 3 g/L [MB] = 96 mg/L Irradiation time: 60 min	83.9	94.9	88.9	~100	Senthilraja et al., 2014
Ce–Ag–ZnO	Sunlight (1.25 × 10^5 lux) Napthol Blue Black (NBB)	Catalyst = 3 g/L [NBB] = 123 mg/L Irradiation time: 40 min	53.0	61.2	60.1	100	Subash et al., 2012
Er-Al–ZnO	18 W LED lamp Methyl Orange (MO)	Catalyst = 1 g/L [MO] = 30 mg/L Irradiation time:	0	~5.0	53.3	98.9	Zhang et al., 2015
Ni–Th–ZnO	300 W Xe lamp Methylene Blue (MB)	Catalyst = 0.375 g/L [MB] = 0.48 mg/L Irradiation time: 180 min	55.0	79.0	65.0	93.0	Vignesh et al., 2014
Zr–Ag–ZnO	Sunlight (1.25 × 10^5 lux) Reactive Red 120 (RR120)	Catalyst = 3 g/L [RR120] = 294 mg/L Irradiation time: 30 min	71.1	71.1	70.6	~100	Subash et al., 2013a
Zr–Ag–ZnO	4 × 8 W medium pressure Hg lamp Acid Black 1 (AB1)	Catalyst = 3 g/L [AB1] = 123 mg/L Irradiation time: 40 min	43.8	59.0	63.9	~100	Subash et al., 2013b

2012), Methylene Blue (Yayapao et al., 2013a) and Methyl Orange (Zhao et al., 2014). The data obtained demonstrated that 1 mol% Nd doped ZnO exhibited highest photodegradation efficiency compared to the other RE-doped ZnOs.

It was also found that the RE-doped ZnO is wide applied in the degradation of Methylene Blue, such as 3 mol% Dy-ZnO (Yayapao et al., 2013b), 4.8 M% ratio Er-ZnO (Yu et al., 2013), 3 mol% Eu-ZnO (Phuruangrat et al., 2014b), 3 mol% Ho (Phuruangrat et al., 2014c) and 1 mol% Nd (Yayapao et al., 2013b). Based on these experimental results, 3 mol% Dy-ZnO irradiated under UV light for 5 h results in the highest photodegradation performance. The photocatalytic degradation of Methyl Orange was studied by employing the ZnO doped with 1 mol% Eu (Zong et al., 2014) and 3 mol% Nd (Zhao et al., 2014) as photocatalysts. The results demonstrated that 1 mol% Eu-loaded ZnO has slightly higher efficiency over 3 mol% Nd-loaded ZnO.

The doped semiconducting catalysts are predicted to exhibit better optical properties, high luminescence properties and high photocatalytic activity in the removal of organic contaminants. This could due to the increased particles surface area, reduced of band gap energy, improved adsorption ability of the particle surfaces and dopant-ZnO interfaces. The optical properties of the photocatalyst is significant for the selection of element for its specific applications. The band gap energy values are important

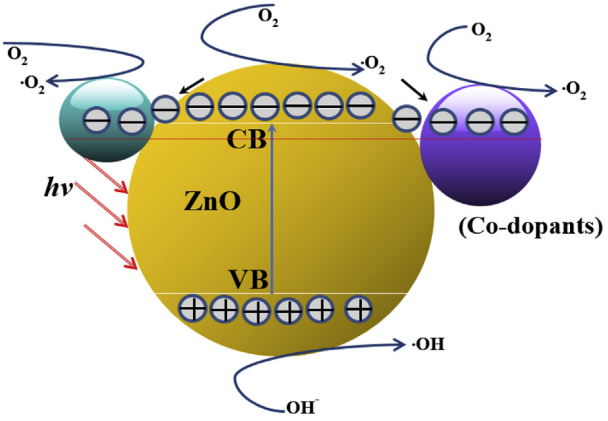

Fig. 6. Mechanism degradation by co-dopants-ZnO system.

in determining the semiconducting ability and also the photocatalytic property of the materials. The doped-ZnO has lower band gap energy values, compared to the individual component of ZnO. The decrease in the band gap is due to the doping of a trace amount of impurity to the ZnO. Under irradiation, more electrons are induced and available in the conduction band. These photogenerated electrons react with oxygen molecules to form superoxide anions. The RE metal on the ZnO surfaces reduced the work function of the adsorbed oxygen interfaces which could improve the oxygen absorption ability. More strong oxidizing species such as hydroxyl, peroxy- and superoxy-radicals are produced and therefore increase the rate of photodegradation of the organic contaminants. The luminescence intensity of the RE-loaded ZnO also enhanced in addition of the RE dopant. The added RE acts as luminescent centers which could effectively improve the luminescence property of the doped ZnO. RE dopants also act as trapping sites for electrons, and thus promote the separation of photogenerated electrons and holes, which leading to high photocatalytic efficiency (Fig. 5).

2.4. Co-dopants

The rapid recombination of the electron–hole pairs can also be countered by the presence of co-dopants (Table 6). It can be seen that the co-doped ZnO has been applied in removing dyes, such as Methylene Blue (Senthilraja et al., 2014; Vignesh et al., 2014), Napthol Blue Black (Subash et al., 2012), Methyl Orange (Zhang et al., 2015), Reactive Red 120 (Subash et al., 2013a) and Acid Black 1 (Subash et al., 2013b). It is obvious that the photodegradation efficiency of co-dopants-ZnO is higher than bare ZnO and single dopant ZnO system. This is due to the co-dopants will simultaneously trapped the photogenerated electron from the conduction band of the ZnO and subsequently reduced the recombination rate of electron–hole (Fig. 6). Therefore, the photoinduced generation of electron–hole pairs will continue and produced a large amount of highly active superoxide radical anions ($O_2^{\cdot-}$) and hydroxyl radicals (•OH), which enhanced the photodecomposition efficiency of the dyes.

2.5. Couple semiconductor

Besides metal doping, coupled semiconductor has been proven to enhance the charge separation of electron–hole pair which

Table 7
Improved photocatalytic efficiency by coupled semiconductor.

Coupling system	Light source/pollutant	Experimental conditions	Photodegradation efficiency (%)		Reference
			ZnO	Binary oxide	
BiOI/ZnO (1:1)	500 W tungsten halogen lamp Methyl Orange (MO)	BiOI/ZnO = 1 g/L [MO] = 10 mg/L Irradiation time = 240 min	2.0	78.0	Jiang et al., 2011
Bi_2O_3/ZnO (1:23)	300 W Xe lamp Rhodamine B (RhB)	Bi_2O_3/ZnO = 1 g/L [RhB] = 4.8 mg/L Irradiation time = 180 min	~15.0	85.0	Yang et al., 2014
Bi_2O_3/ZnO (1 at.%)	55 W compact fluorescence lamp Phenol	Bi_2O_3/ZnO = 1 g/L [Phenol] = 19.8 mg/L Irradiation time = 360 min	56.4	98.4	Lam et al., 2013b
Bi_2O_3/ZnO (11.7 wt.% Bi_2O_3)	4 × 8 W medium pressure Hg lamp Acid Black 1 (AB1)	Bi_2O_3/ZnO = 4 g/L [AB1] = 185 mg/L Irradiation time = 90 min	78.0	~100	Balachandran and Swaminathan, 2012
CdO/ZnO (5 wt.% CdO)	250 W projection lamp Methylene Blue (MB)	CdO/ZnO = N/A [MB] = 9.6 mg/L Irradiation time = 360 min	0	100	Saravanan et al., 2011
CdO/ZnO (20% CdO)	Solar simulator Methylene Blue (MB)	CdO/ZnO = 0.4 g/L [MB] = 3.2 mg/L Irradiation time = 240 min	The rate of degradation is 7.1×10^4 min^{-1}	The rate of degradation is 27×10^4 min^{-1}	Samadi et al., 2014
CdS/ZnO (1:3)	300 W Xe lamp Rhodamine B (RhB)	CdS/ZnO = 0.5 g/L [RhB] = 24 mg/L Irradiation time = 90 min	~45.0	100	Lai et al., 2011a
CeO_2/ZnO (1:5)	8 W UV light Rhodamine B (RhB)	CeO_2/ZnO = 0.5 g/L [RhB] = 24 mg/L Irradiation time = 180 min	82.3	98	Li et al., 2011b
CeO_2/ZnO (10% CeO_2)	18 W Hg lamp Methylene blue (MB)	CeO_2/ZnO = 0.1 g/L [MB] = 10 mg/L Irradiation time = 150 min	52.3	67.4	Liu et al., 2014
CuO/ZnO	15 W UV tube Methyl Orange (MO)	CuO/ZnO = 2 g/L [MO] = L/L Irradiation time = 60 min	50.0	90.0	Liu et al., 2008
CuO/ZnO (8 mol% CuO)	150 W Tungsten halogen lamp Acid Red 88 (AR88)	CuO/ZnO = 1.4 g/L [AR88] = L/L Irradiation time = 60 min	The rate of degradation is 0.63×10^{-3} s^{-1}	The rate of degradation is 1.43×10^{-3} s^{-1}	Sathishkumah et al., 2011
CuO/ZnO (1:2)	300 Xe lamp Rhodamine B (RhB)	CuO/ZnO = 0.3 g/L [RhB] = 24 mg/L Irradiation time = 120 min	37.0	100	Li et al., 2010
Cu_2O/ZnO (1.5 M Cu_2O)	200 W tungsten halogen lamp Methyl Orange (MO)	Cu_2O/ZnO = 1 g/L [MO] = 25 mg/L Irradiation time = 180 min	30.0	73.0	Xu et al., 2010
Cu_2O/ZnO (70% Cu_2O)	500 W tungsten halogen lamp Orange II (OII)	Cu_2O/ZnO = 0.5 g/L [OII] = 10 mg/L Irradiation time = 60 min	No decolourization	The rate of degradation is 14.97×10^{-3} min^{-1}	Helaïli et al., 2010
α-Fe_2O_3/ZnO (0.5 wt.% α-Fe_2O_3)	500 W medium pressure Hg lamp Dichloro acetic acid (DCA)	α-Fe_2O_3/ZnO = 1 g/L [DCA] = 5 mmol Irradiation time = 120 min	15.0	55.0	Sakthivel et al., 2002
Fe_3O_4/ZnO (1:10)	30 W UV light Methyl Orange (MO)	Fe_3O_4/ZnO = 1.5 g/L [MO] = L/L Irradiation time = 360 min	55.0	83.0	Hong et al., 2008
Fe_3O_4/ZnO (1:4)	575 W metal halide lamp Phenol	Fe_3O_4/ZnO = 0.325 g/L [Phenol] = N/A Irradiation time = 150 min	52.0	82.8	Feng et al., 2014
Fe_3O_4/ZnO (10 wt.% Fe_3O_4)	500 W high pressure Hg lamp Methyl Orange (MO)	Fe_3O_4/ZnO = 0.5 g/L [MO] = 19.6 mg/L Irradiation time = 60 min	85.0	93.6	Xia et al., 2011
GO/ZnO	300 W Xe light Methylene Blue (MB)	GO/ZnO = 0.8 g/L [MB] = 9.6 mg/L Irradiation time = 40 min	25.0	100	Li et al., 2012a
GO/ZnO	10 × 10 LED lamp Methylene Blue (MB)	GO/ZnO = 1 g/L [MB] = 8 mg/L Irradiation time = 60 min			Dai et al., 2014
MoO_3/ZnO (1 at.%)	55 W compact fluorescence lamp 2,4-dichloro-phenoxyacetic acid (2,4-D)	MoO_3/ZnO = 1 g/L [2,4-D] = L/L Irradiation time = 360 min	56.4	98.4	Lam et al., 2013c
$NaNbO_3$/ZnO (10 wt.%)	2 × 125 W Hg lamp Methylene Blue (MB)	$NaNbO_3$/ZnO = 1 g/L [MB] = 10 mg/L Irradiation time = 60 min	80.0	~100	Xu et al., 2011
Nb_2O_5/ZnO	Natural sunlight Phenol	Nb_2O_5/ZnO = 1 g/L [Phenol] = L/L Irradiation time = 40 min	57.8	100	Lam et al., 2014
RGO/ZnO	150 W Hg lamp Rhodamine 6G (Rh6G)	RGO/ZnO = 0.1 g/L [Rh6G] = 10 mg/L Irradiation time = 10 min	~55.0	~100	Zhang et al., 2014a

Table 7 (*continued*)

Coupling system	Light source/pollutant	Experimental conditions	Photodegradation efficiency (%)		Reference
			ZnO	Binary oxide	
RGO/ZnO (1:2)	12 W UV lamp Methylene Blue (MB)	RGO/ZnO = 0.4 g/L [MB] = 9.6 mg/L Irradiation time = 150 min	15.0	90.0	Zhou et al., 2012
SiO_2/ZnO (5 wt.%)	UV light Rhodamine B (RhB)	SiO_2/ZnO = N/A [RhB] = 4.8 mg/L Irradiation time = 100 min	47.0 (pH 10.5)	93.0 (pH 10.5)	Zhai et al., 2010
SnO_2/ZnO (5 wt.%)	8 W UV light Acid Orange 10 (AO10)	SnO_2/ZnO = 5 g/L [AO10] = 226.2 mg/L Irradiation time = 60 min	84.0	100	Kuzhalosai et al., 2013
SnO_2/ZnO (1:2)	4 × 40 W UV lamp Methyl Orange (MO)	SnO_2/ZnO = 1.33 g/L [MO] = L/L Irradiation time = 100 min	~35.0	~60.0	Yang et al., 2010
SnO_2/ZnO (1:1)	125 W high pressure Hg lamp Methylene Blue (MB)	SnO_2/ZnO = 1 g/L [MB] = 10 mg/L Irradiation time = 40 min	80.0	100	Uddin et al., 2012
TiO_2/ZnO	UV lamp Methylene Blue (MB)	TiO_2/ZnO = 0.8 g/L [MB] = 10 mg/L Irradiation time = 180 min	35.0	70.0	Pant et al., 2012
TiO_2/ZnO (80:20)	16 W UV-B lamp 4-chlorophenol (4CP)	TiO_2/ZnO = 2 g/L [4CP] = 25 mg/L Irradiation time = 75 min	75.0	100	Pozan and Kambur, 2014
WO_3/ZnO (2 at.%)	15 W UV light Acid Orange II (AOII)	WO_3/ZnO = 0.625 g/L [AOII] = L/L Irradiation time = 300 min	41.0	66.0	Yu et al., 2011
WO_3/ZnO (2 at.%)	55 W compact fluorescence lamp Resorcinol (ReOH)	WO_3/ZnO = 1 g/L [ReOH] = 19.8 mg/L Irradiation time = 180 min	70.0	100	Lam et al., 2013a
ZnO_2/ZnO (75:25)	8 × 12 W UV light Methyl Orange (MO)	ZnO_2/ZnO = 0.25 g/L [MO] = 37.5 mg/L Irradiation time = 120 min	20.0	45.0	Hsu and Wu, 2005
ZrO_2/ZnO	15 W Hg lamp Dimethyl phthalate (DMP)	ZrO_2/ZnO = 1 g/L [DMP] = 50 mg/L Irradiation time = 60 min	40.0	80.0	Liao et al., 2010
ZrO_2/ZnO (1:2)	8 × 8 W low pressure Hg lamp 2,4-dichloro-phenol (2,4-DCP)	ZrO_2/ZnO = 0.3 g/L [2,4-DCP] = 75 mg/L Irradiation time = min	The rate of degradation is 0.39 h^{-1}	The rate of degradation is 0.45 h^{-1}	Sherly et al., 2014

increase the lifetime of the charge carriers and consequently reduce the recombination of electron–hole (Serpone et al., 1995). Table 7 shows the enhancement in photodegradation efficiency by ZnO coupling system. Methylene Blue, a cationic dye is widely chosen as the model organic pollutant for the photocatalytic degradation by using ZnO coupling system, such as CdO/ZnO (Saravanan et al., 2011; Samadi et al., 2014), CeO_2/ZnO (Liu et al., 2014), GO/ZnO (Li et al., 2012a; Dai et al., 2014), $NaNbO_3$/ZnO (Xu et al., 2011), RGO/ZnO (Zhou et al., 2012), SnO_2/ZnO (Uddin et al., 2012) and TiO_2/ZnO (Pant et al., 2012). It can be seen from Table 7 that graphene oxide (GO) coupled with ZnO shows the highest photodegradation efficiency among the studied coupling system. Similarly, enhanced photocatalytic activity was also observed in the removal of Methyl Orange (MO) by BiOI/ZnO (Jiang et al., 2011), CuO/ZnO (Liu et al., 2008), Cu_2O/ZnO (Xu et al., 2010), Fe_3O_4/ZnO (Hong et al., 2008a; Xia et al., 2011), SnO_2/ZnO (Yang et al., 2010) and ZnO_2/ZnO (Hsu and Wu, 2005). The decolorization percentage of Rhodamine B (RhB) increased at least twice when Bi_2O_3/ZnO (Yang et al., 2014), CdS/ZnO (Li and Wang, 2011a), CuO/ZnO (Li and Wang, 2010) and SiO_2/ZnO (Zhai et al., 2010) was applied as the photocatalyst. Nevertheless, only 16% enhancement was observed with CeO_2/ZnO (Li et al., 2011b). The photocatalytic activities of some semiconductors coupled with ZnO have been studied for phenol (Lam et al., 2013b; Feng et al., 2014; Lam et al., 2014), Acid Black 1 (AB1) (Balachandran and Swaminathan, 2012), Acid Red 88 (AR88) (Sathishkumah et al., 2011), Orange II (OII) (Helaïli et al., 2010), dichloroacetic acid (DCA) (Sakthivel et al., 2002), 2,4-dichlorophenoxy-acetic acid (2,4-D) (Lam et al., 2013c), Rhodamine 6G (Rh6G) (Zhang et al., 2014a), Acid Orange 10 (AO10) (Kuzhalosai et al., 2013), 4-chlorophenol (4-CP) (Pozan and Kambur, 2014), Acid Orange II (AOII) (Yu et al., 2011), resorcinol (ReOH) (Lam et al., 2013a), dimethyl phthalate (DMP) (Hsu and Wu, 2005) and 2,4-dichlorophenol (2,4-DCP) (Liao et al., 2010).

Fig. 7 illustrates the band structure of a composite photocatalyst, prepared by a mixture of wide- and narrow-band-gap photocatalysts. Upon light irradiation, the photogenerated electrons can flow from one semiconductor with a higher conduction band minimum to the other with a lower conduction band minimum. Moreover, the formation of heterojunction led to a more efficient interelectron transfer between the two catalysts. In this way, the photoinduced electron–hole pairs were separated and the probability of electrons–holes pair's recombination was reduced (Shang et al., 2009; Wang et al., 2009b; Peng et al., 2010). Thus, the photocatalytic activity was enhanced.

From Table 7, we can conclude that the comparison of photocatalytic activity for different types of coupling system is difficult. This is due to the fact that the photoactivity of catalysts is strongly depend on its band gap, morphology, particle size, porosity, surface area and surface hydroxyl density. Moreover, the irradiation intensity and photoreactor design also play a crucial role in

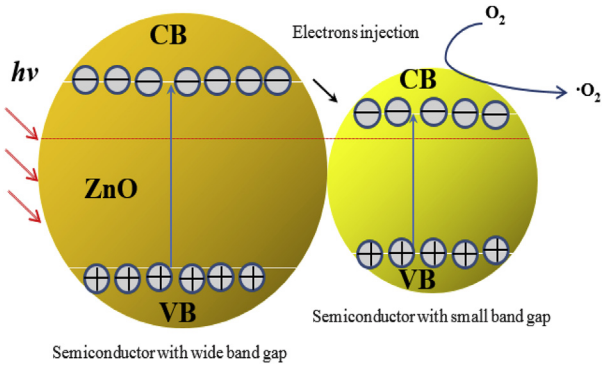

Fig. 7. The band structure of a composite photocatalyst, prepared by a mixture of wide- and narrow-band-gap photocatalysts.

determining the performance of a photocatalyst.

3. Factors affecting photodegradation efficiency

3.1. ZnO loading

Most of the studies have investigated the effect of catalyst loading on the photocatalytic efficiency (Mrowetz and Selli, 2006; Kositzi et al., 2007; Chatzitakis et al., 2008; Lu et al., 2009; Hayat et al., 2011). These results indicated that the photodegradation rate initially increases with increasing in the amount of catalyst loaded until it reached an optimum mass. This phenomenon is based on the fact that an increase in the catalyst dosage will enhance the total active surface area and the number of reaction sites on the catalyst surface. As a result, the number of hydroxyl and superoxide radicals increased as well, which facilitates the degradation of the organic pollutants. Thus, the degradation percentage was enhanced. However, the percentage of photodegradation decreases at higher loadings when the photocatalyst dosage was beyond the optimum concentration due to light scattering and screening effects. Moreover, high catalyst dosage facilitates agglomeration (particle–particle interaction) leading to a reduction in catalyst surface area available for light absorption and pollutant adsorption, which in turn, reduced the photocatalytic efficiency. On the other hand, one should also noticed that the solution turbidity increase as well. This phenomenon inhibits the penetration of light into the solution. Thus, the photoactivated volume of the suspension decreases and consequently lowers the degradation rate. These suggested that an optimum catalyst mass should be obtained in order to avoid usage of excess catalyst and to ensure a maximum absorption of photons.

3.2. ZnO structure

The photodegradation efficiency can be improved through the advancement in the ZnO structure. Recently, ZnO nanostructure received a great interest in the photocatalytic study due to their unique structures and properties. The nanostructured ZnO can exists in various morphologies such as nanorods, nanowires, nanosheets, nanodumbbells, nanobelts, nanotetrapods, nanoflowers and nanospiral disks, where are different from the bulk ZnO (Lai et al., 2010; Saravanan et al., 2011). Nanostructured ZnO have a size in nanoscale with higher surface area. A high surface-to-volume ratio offers better physicochemical properties. Nano ZnO possesses better surface effect and quantum effect (Lai et al., 2010). One dimensional ZnO nanorods were used in the photodegradation of Methylene Blue. The study indicated that the ZnO nanorods with higher specific surface area produces better photodegradation efficiency compared to the nanorods with lower surface area (Assi et al., 2015). A novel sphere of ZnO nanosheets was constructed for the photodegradation of Rhodamine B. This three-dimensional (3D) fluffy structure offers a large surface area with more active sites for reaction. The photocatalytic removal of Rhodamine B indicated a higher rate of degradation compared to other nanostructures due to the larger specific surface area and improved segregation efficiency for electrons and holes (Lai et al., 2010).

3.3. Substrate concentration

Many reports have showed that the concentration of organic contaminants in aqueous solution has a detrimental effect on the photocatalytic degradation rate (Rabindranathan et al., 2003; Akyol and Bayramoğlu, 2005; Sirtori et al., 2006; Mahalakshmi et al., 2007; Wu et al., 2010). The degradation efficiency reduced when the substrate concentration increased. This is due to the fact that as the concentration of the target pollutant increases, more and more organic substances are adsorbed on the catalyst surface. Therefore, the demand of oxidizing species (•OH and $\cdot O_2^-$) for the degradation of the organics also increases. However, the number of active sites on the catalyst surface remains constant for a fixed catalyst dosage, light intensity and irradiation period. Therefore, the generation of hydroxyl radicals is insufficient since there are only a few active sites available for the adsorption of hydroxyl ions. Furthermore, the photons get intercepted before they can reach to the catalyst surface at higher pollutant concentrations. The competitive consumption of hydroxyl radicals by the generated intermediates reduces the percentage of degradation in highly concentrated pollutant solution.

3.4. Solution pH

Solution pH plays a vital role in photocatalytic water system. pH not only affects the surface charge of the catalyst particles (Haque et al., 2006), but also influences the positions of conduction and valence bands in a semiconductor (Chong et al., 2010). Moreover, industrial wastewater may be discharged at various pH, which make the photocatalytic process more complicated. Generally, an organic compound is neutral when pH of solution is lower than its pK_a value. When the pH of solution is greater than the pK_a value, the compound deionized and exists as negatively charge species. In addition, the solution pH has an impact on the electrostatic interaction between a catalyst surface, solvent molecules, substrate and charged radicals formed during photodegradation process. Recently, Kosmulski (2006) reported an update of the points of zero charge (pzc) for some semiconductors. The protonation and deprotonation of organics and photocatalyst surface could occur either in acidic or in alkaline conditions as shown in the following reactions (Eqs. (20) and (21)):

$$\mathrm{pH} < \mathrm{pzc} : \mathrm{MOH} + \mathrm{H^+} \rightarrow \mathrm{MOH_2^+} \quad (20)$$

$$\mathrm{pH} > \mathrm{pzc} : \mathrm{MOH} + \mathrm{OH^-} \rightarrow \mathrm{MOH^-} + \mathrm{H_2O} \quad (21)$$

Therefore, the semiconductor surface is positively charged below its pzc value and is negatively charged when exceeded its pzc. According to Shifu and Gengyu (2005), the photogenerated holes (h^+) are the predominant oxidizing species at low pH, whereas at neutral or alkaline medium, hydroxyl radicals play the major role in oxidizing the organic contaminants. However, it should also be noticed that hydroxyl radicals are rapidly scavenged at high pH due to abundance of hydroxyl ions which inhibits its reaction with the pollutant substrate (Davis and Huang, 1989).

Thus, suitable pH should be carefully selected to ensure an efficient photocatalytic degradation process.

3.5. Light intensity

Photocatalytic reaction rate depends on the light absorption by a photocatalyst in photocatalytic process. It is believed that more radiations fall on the catalyst surface at higher light intensity and hence more hydroxyl radicals are produced, which in turn increases the reaction rate (Shafaei et al., 2010; Mahalakshmi et al., 2007; Behnajady et al., 2006). Moreover, it controls the formation of electron–hole pairs in the photocatalysis process. Herrmann (1999) concluded that the reaction rate was proportional to the radiant flux, φ for $\varphi < 25$ mW cm^{-2}, but varied to square-root dependency ($\varphi^{0.5}$) when φ above 25 mW cm^{-2}. In an n-type semiconductor such as ZnO and TiO_2, the number of photo-induced holes in valence band is much less than the photo-generated electrons in conduction band. This indicated that the photo-generated holes are the limiting active species (Malato et al., 2009). At much higher light intensities, the photodegradation rate is independent to the radiant flux (φ^0). Under this condition, the reaction rate only depends on the mass transfer within the reaction. This is due to the catalyst surface was fully covered by the saturated solids, which limits the mass transfer for both adsorption and desorption. Thus, the reaction rate remains constant despite an increase in the light intensity.

3.6. Light wavelength

For UV irradiation, its corresponding electromagnetic spectrum can be classified as UV-A, UV-B and UV-C, according to its emitting wavelength. The UV-A range has its light wavelength spans from 315 to 400 nm (3.10–3.94 eV), while UV-B has wavelength range of 280–315 nm (3.94–4.43 eV) and the germicidal UV-C ranges from 100 to 280 nm (4.43–12.4 eV) (Rincon and Pulgarin, 2005). Ochuma et al. (2007) reported that the UV-A light provides light photons sufficient for photonic activation of the prepared TiO_2 in the photodegradation of 1,8-diazabicyclo[5.4.0]undec-7-ene. Generally, the photocatalytic efficiency is higher at 254 nm radiation due to shorter penetration capability of the higher energy photon, which increased the number of electron–hole pairs generated for the decomposition of the target pollutant (Bayarri et al., 2007). However, Venkatachalam et al. (2007), in photodegradation of 4-chlorophenol, found a lower degradation efficiency at 254 nm and attributed it to light wasting and partial absorption by 4-chlorophenol itself.

3.7. Temperature

Photocatalytic degradation process can be operated at ambient temperature and atmospheric pressure due to photonic activation. This is beneficial for water purification treatment whereby the heating step can be excluded to conserve energy. The optimum temperature for photocatalytic process is in the range of 20–80 °C with a few kJ/mol of activation energy (Malato et al., 2003). In general, an increase in the reaction temperature may enhance the degradation rate of the organic contaminants, however it may also reduce the adsorptive capacities of the reactant species and dissolved oxygen, which resulted in lower photodegradation efficiency (Herrmann, 1999; Gaya and Abdullah, 2008; Chatzitakis et al., 2008; Kositzi et al., 2007). This is confirmed by Van't Hoff–Arrhenius equation, where the chemical reaction rate constant, k is linearly proportional to exp (−1/T).

3.8. Inorganic species

Most of the scientific works indicated that the major energy wasting step in the photocatalytic reaction is the electron–hole recombination that prompts low quantum yield. Therefore, the recombination of electron–hole pairs must be prevented to ensure the photocatalytic process to work more effective. The addition of inorganic oxidants improves the photodegradation rate by: 1) Increasing the number of trapped electrons to avoid recombination of electron–hole pair; 2) Generating more radicals and other oxidizing species to oxidize the generated reactive intermediates; 3) Increasing the concentration of hydroxyl radicals and oxidation rate of intermediate compounds and 4) Avoiding problems caused by low oxygen concentration (Wei et al., 2009; Selvam et al., 2007; Singh et al., 2007).

Several inorganic oxidants were studied for their influences towards the photocatalytic efficiency of ZnO photocatalyst, such as H_2O_2, $S_2O_8^{2-}$, BrO_3^-, and SO_3^-. Hydrogen peroxide, H_2O_2, a powerful oxidizing species and electron acceptor which leading to the increased in the rate of photodegradation of various organics. Upon photoexcitation, electrons and holes were generated on the surface of ZnO photocatalyst. The generated holes and electrons will involve in the production of strong oxidizing radicals, which are the main species that responsible for the destruction of organic pollutants. H_2O_2 accepts a photoinduced electron from the conduction band and form the hydroxyl radical via the redox reaction on the catalyst surface (Eq. (22)). H_2O_2 can also split photolytically to hydroxyl radicals directly as illustrated in Eq. (23) (Dixit et al., 2010):

$$H_2O_2 + e_{CB}^- \rightarrow \cdot OH + OH^- \quad (22)$$

$$H_2O_2 + h\nu \rightarrow 2 \cdot OH \quad (23)$$

The hydroxyl radicals that formed on the ZnO surface are capable of oxidizing various organic compounds into less hazardous molecules such as H_2O, CO_2 and inorganic salts. It was reported that the photodegradation efficiency reached an optimum condition when a trace amount of H_2O_2 is used in the presence of ZnO (Khattab et al., 2012; Shanthi and Kuzhalosai, 2012). However, it is worth to pinpoint that the excessive amount of H_2O_2 will suppress the photodegradation rate by acts as hydroxyl radical or hole scavenger to form perhydroxyl radicals (HO_2•), which is a much weaker oxidant than hydroxyl radicals (•OH) as demonstrated by reactions (Eqs. (24) and (25)). Therefore, a proper amount of hydrogen peroxide is essential in order to improve the photodegradation efficiency (Yusoff et al., 2014).

$$H_2O_2 + \cdot OH \rightarrow HO_2 \cdot + H_2O \quad (24)$$

$$H_2O_2 + h_{VB}^+ \rightarrow H^+ + HO_2 \cdot \quad (25)$$

The addition of bromate ions, BrO_3^- is beneficial to enhance the photodegradation percentage of organic contaminants, by forming BrO_2^- and HOBr (Eqs. (26) and (27)), which reduces the recombination rate of the electron–hole pairs (Seyed-dorraji et al., 2009).

$$BrO_3^- + 2H^+ + e_{CB}^- \rightarrow BrO_2 \cdot + H_2O \quad (26)$$

$$BrO_3^- + 6H^+ + 6e_{CB}^- \rightarrow Br^- + 3H_2O \quad (27)$$

The presence of persulfate ions, $S_2O_8^{2-}$ in the photocatalytic system showed higher degradation rate by promoting the charge separation and also generating the sulphate radical anion ($SO_4^{\cdot -}$), which is a very strong oxidizing agent that mineralize a wide range of organic pollutants (reduction potential of $SO_4^{\cdot -} = +2.60$ V). The

generated $SO_4^{\cdot-}$ will then reacts with the water molecule to form hydroxyl radicals (Hazime et al., 2014) (Eqs. (28)–(31)).

$$S_2O_8^{2-} + e_{CB}^- \rightarrow SO_4^{\cdot-} + SO_4^{2-} \quad (28)$$

$$SO_4^{2-} + \cdot OH \rightarrow SO_4^{\cdot-} + OH^- \quad (29)$$

$$SO_4^{2-} + h_{VB}^+ \rightarrow SO_4^{\cdot-} \quad (30)$$

Oxone, SO_3^- a strong oxidant that intend to react with the electrons from the conduction band of ZnO to form sulphate radicals ($SO_4^{\cdot-}$) and hydroxyl radicals under light induction Eqs. (31) and (32). The sulphate radicals are easily react with hydroxyl species from water and thus capable of improving the degradation efficiency (Krishnakumar et al., 2010).

$$HOOSO_3^- + e_{CB}^- \rightarrow SO_4^{\cdot-} + OH^- \quad (31)$$

$$HOOSO_3^- + e_{CB}^- \rightarrow SO_4^{2-} + \cdot OH \quad (32)$$

Some inorganic ions/electrolytes will tend to retard the photodegradation of ZnO. It was demonstrated that inorganic ions such as Na_2SO_4, NaCl, $NaNO_3$ and Na_2CO_3 tend to retard the photodegradation (Krishnakumar et al., 2010). These ions could be deposited on the ZnO surface and the inorganic ions inhibited the degradation. This could be attributed by the blocking of active sites on the surface of ZnO. For example, the inclusion of NaCl retard photodegradation of ZnO which could due to the radical scavenging effect of chloride as described in Eqs. (33) and (34) (Assi et al., 2015).

$$Cl^- + \cdot OH \rightarrow HOCl\cdot^- \quad (33)$$

$$HOCl\cdot + H^+ \rightarrow Cl\cdot + H_2O \quad (34)$$

The photodegradation decreases with increase of Cl concentration, which is similar to the negative effect caused by CO_3^{2-} and HCO_3^- as follows:

$$CO_3^{2-} + \cdot OH \rightarrow OH^- + CO_3\cdot^- \quad (35)$$

$$HCO_3^- + \cdot OH \rightarrow H_2O + CO_3\cdot \quad (36)$$

This is will pose a major challenge for treating industrial wastewater that may contain high impurities of anion inhibitors such as Cl and CO_3 anions.

4. Advancement of ZnO in removing contaminants

Phenolic compounds, persistent organic pollutants (POPs) and dyes are among the most toxic organic compounds have long been a focus of concern due to their gravest threat to human health, marine life and environment. The importance of the removal of organic pollutants in industries wastewater arises due to the toxicity of these pollutants, and their ability to bioaccumulate in the aquatic life and slowly moving to the food chain. Multiple methods have been developed and used to remove the organic pollutants. However, most of these methods require complicated/time-consuming procedure, highly precise sample preparation, expensive or sophisticated instruments, have poor removal efficiency and long turnaround times which make those methods unsuitable for field applications. The ability of advanced photodegradation technology to remove POPs as well as dyes and phenolic compounds in wastewater has been widely applied. This technology is progressively being used in many industries and even being commercialized in many countries. ZnO has been an attractive candidate as a photocatalyst to selectively remove pollutants due to its photosensitivity and low in price. Photodegradation of organic pollutants using ZnO photocatalyst demonstrates a simple, versatile and cost effective treatment technology. Many literature have proven that the decreased in the concentration of the contaminants when ZnO is used as a photocatalyst when illuminated by UV or visible lights. The efficiency application of ZnO in photodegradation to remove phenolic compounds, POPs and dyes is presented in the Table 8.

4.1. Phenolic compounds

Phenol and its derivatives are one of the most important environmental pollutants which are mainly discharged from textile industries, petrochemical plants, and petroleum refineries. In recent years, widespread pollution of phenolic compounds in aquatic ecosystem is one of the critical environmental issue. Phenolic pollutants are very toxic which can cause lethal for aquatic life even in a low concentration. Wastewaters which containing a significant amount of phenolic compounds should be treated before being discharged to the environment. Some conventional methods such as chemical coagulation, solvent extraction, adsorption, and biological treatment have limitations in treating the phenolic wastewater. Advanced oxidation process (AOP) offers better advantage in removing of phenolic compounds over conventional methods. Photocatalysis is one of the AOPs which possesses great potential in treating various organic pollutants, including phenolic pollutants. The use of photocatalytic elimination of phenolic compounds has been carried by Selvam et al. (2007). ZnO, a semiconductor with photocatalytic property was used to detoxify the toxic 4-fluorophenol (4FP) in the studies (Table 8). Mercury lamp is used as a light source, which create electron hole pairs in the ZnO after the photoexcitation. Gaya et al. (2009) successfully demonstrated the photocatalytic ability of ZnO to remove 4-chlorophenol (4CP). The source of light was ultraviolet-A (UV-A) and 4CP was completely degraded after 180 min of irradiation.

4.2. Persistent organic pollutants (POPs)

Persistent organic pollutants (POPs) are harmful chemicals that will detrimental affect the environment and human health. The major concern of POP is because they remain for long periods of time in the environment. Therefore, it will bioaccumulate and transport from lower food chain to the higher food chain. Example of these pollutants is fungicides, herbicides, insecticides, and pesticides. As shown in Table 8, these POPs can also be degraded by ZnO under UV light irradiation. Mijin et al. (2009) has also successfully degraded metamitron which is mainly used as herbicides by using ZnO under 300 W of UV light irradiation. The harmful pesticide e.g. dimethoate was completely degraded just within 60 min by ZnO under 125 W UV light (Evgenidou et al., 2005b). The presence of pharmaceutical compounds which is a potential endocrine disrupting compound (EDC) has becoming major concern. Although the impact of these pharmaceutical compounds on human health is unclear, it causes adverse effects on aquatic life. These pharmaceutical compounds such as amoxicillin, amplicillin, cloxacillin, and tetracycline have been degraded by applying ZnO as photocatalyst under UV or solar light irradiation (Elmolla and Chaudhuri, 2010, Palominos et al., 2009). Lastly, ZnO has proven to be a potential photocatalyst to treat various type of organic pollutants under UV and solar irradiation.

Table 8
Photocatalytic degradation of selected organic contaminants by ZnO.

Pollutant	Experimental conditions	Degradation rate	Reference
Phenolics			
4-fluorophenol (4FP)	4 × 8 W medium pressure Hg lamp, light intensity = 1.381×10^{-3} Einstein L^{-1} s^{-1}, ZnO = 2 g/L, C_0 = 100 mg/L	Highest decomposition of 4FP was observed at pH 7 with 0.0325 min^{-1} in rate. Mg^{2+} showed greatest photoactivity among tested transition metal ions (Fe^{2+}, Fe^{3+}, Cu^{2+} and Mg^{2+}).	Selvam et al., 2007
4-chlorophenol (4CP)	6 W UV-A lamp, ZnO = 2 g/L, C_0 = 50 mg/L	4CP was completely degraded after 180 min irradiation. Cl^-, SO_4^{2-} and $S_2O_8^{2-}$ showed enhancement in the reaction rate at pH 7 whereas HPO_4^{2-} retarded the process.	Gaya et al., 2009
Phenylhydrazine	75 W medium pressure Hg lamp, ZnO = 0.25 g/L, C_0 = 20 mg/L	Degradation efficiency of 37% achieved in 180 min irradiation.	Nezamzadeh-Ejhieh and Khodabakhshi-Chermahini, 2014
Ortho-nitrophenol	30 W UV-C lamp, ZnO = 0.25 g/L, C_0 = 10 mg/L	Degradation efficiency of 98% achieved in 300 min irradiation.	Assi et al., 2015
Fungicides			
2-phenylphenol (OPP)	200 W high pressure mercury lamp (λ > 300 nm), ZnO = 2 g/L, $C_0 = 5.0 \times 10^{-4}$ M	Most of OPP was removed after 7 h of irradiation with rate = 9.7×10^8 mol^{-1} L s^{-1}. Additional of Cl^-, SO_4^{2-}, NO_3^-, ethanol and *tert*-butanol affects the photodegradation of OPP.	Khodja et al., 2001
Herbicides			
Metamitron	300 W lamp (mix of lights, UV-A:UV-B = 13.6:3), ZnO = 2 g L^{-1}, C_0 = 9 mg/L	100% removal was observed in 240 min with rate = 0.0531 min^{-1}. After 4 h, only 56% elimination in TOC.	Mijin et al., 2009
Insecticides			
Diazinon	30 W (UV-C) Hg lamp, light intensity = 11.2 W m^{-2}, ZnO = 0.15 g/L, C_0 = L/L	The synthesized ZnO was superior to decomposition of diazinon compared to commercial ZnO (Merck) with 80% removal in 80 min.	Daneshvar et al., 2007
Dichlorvos	125 W high pressure Hg lamp (λ > 290 nm), ZnO = 0.5 g/L, C_0 = 22 mg/L	Complete degradation was achieved after 3 h of light exposure, while only 32% reduction in DOC after 6 h irradiation.	Evgenidou et al., 2005a
Imidacloprid	Natural solar irradiation	Degradation efficiency of 37.4% after 60 min irradiation.	Zsigmond, 2014
Pesticides			
Dimethoate	125 W high pressure Hg lamp (λ > 290 nm), ZnO = 0.1 g/L, C_0 = 10 mg/L	Complete disappearance of dimethoate was observed in 60 min. The addition of H_2O_2 has no effect on the removal efficiency, while the presence of $K_2S_2O_8$ enhanced the reaction rate.	Evgenidou et al., 2005b
Pharmaceuticals			
Amoxicillin (AMX), Ampicillin (AMP), Cloxacillin (CLX)	6 W UV lamp (λ = 365 nm), ZnO = 0.5 g/L, C_0 = 100 mg/L	Under optimisation conditions at pH 11, AMX, AMP and CLX achieved 100% removal in 180 min with rate = 0.018, 0.015 and 0.029 min^{-1}, respectively.	Elmolla and Chaudhuri, 2010
Tetracycline (TC)	Xe lamp (λ = 300–800 nm), light intensity = 250 W m^{-2}, ZnO = 1 g L^{-1}, C_0 = L/L	After 15 min irradiation at pH 11, all TC fully decomposed. However, total mineralisation occurred only after 45 min irradiation.	Palominos et al., 2009
Dyes			
(a) Anionic dyes			
Acid Red 18 (AR18)	8 × 8 W medium pressure Hg lamps (λ = 365 nm), ZnO = 4 g/L, $C_0 = 5 \times 10^{-4}$ M	Complete dye removal occurred after 60 min irradiation. However, degradation reached 100% only after 120 min.	Sobana and Swaminathan, 2007
Methyl Orange (MO)	125 W high pressure Hg lamp (λ = 365 nm), ZnO = 1 g/L^{-1}, C_0 = L/L	ZnO with rugby structure displayed highest removal efficiency with nearly total decolourisation within 2 h.	Xie et al., 2011
Orang II (OII)	18 W BLB T8 UV lamp (λ = 315–400 nm) ZnO = 0.5 g L^{-1}	Photodegradation efficiency of 100% achieved after 60 min irradiation.	Siuleiman et al., 2014
(b) Cationic dyes			
Acridine Orange (AO)	500 W halogen lamp, light intensity = 17,500 lux, ZnO = 5 g/L, $C_0 = 2.0 \times 10^{-5}$ M	Complete decolourisation was achieved after 180 min irradiation. The presence of surfactants (SDS and CTAB) decreased the reaction rate.	Pare et al., 2008
Methyl Green (MG)	2 × 15 W visible lamps, light intensity = 4.8 W m^{-2}, ZnO = 0.25 g/L, C_0 = 50 mg/L	Complete colour removal obtained at pH 10 after 16 h. Additional of Cl^- and CO_3^{2-} negatively affect the degradation rate, while $S_2O_8^{2-}$ and H_2O_2 at optimum concentration showed enhancement in decolourisation.	Mai et al., 2008
Methylene Blue (MB)	500 W tungsten-halogen light intensity = 1060 W m^{-2}, ZnO 20 mM	Degradation efficiency of 80% achieved after 180 min irradiation.	Danwittayakul et al., 2015

4.3. Dyes

Dyes are one of the most important pollutants from the textile industry. Synthetic dyes such as Methyl Orange, Methylene Blue and Methyl Green are mainly used in the paper and textile industries. Several methods have been applied to reduce the impact of these synthetic dyes on aquatic life and environment. Unfortunately, many conventional methods such as membrane

separation, adsorption and biological treatments required high operating cost and have insufficient removal efficiency. Recently, photodegradation based on the photocatalytic reaction has been proposed as an efficient method for the removal of pollutants including dyes. ZnO is among the most popular photocatalyst has been widely used to remove dyes due to its ability to absorb a wide solar spectrum. The successful photodegradation using ZnO in treating Methylene Blue was demonstrated by Danwittayakul et al. Degradation efficiency of 80% was achieved after 180 min of irradiation with a light intensity of 1060 W m^{-2} (Danwittayakul et al., 2015). ZnO was applied to degrade Orange II under UV illumination. 100% of photodegradation efficiency was achieved after 60 min of irradiation (Siuleiman et al., 2014). The degradation of Methyl Green was examined with a completely color removal after 16 h at pH 10 by visible light with an intensity of 4.8 W m^{-2}. (Mai et al., 2008). ZnO has also found to achieve satisfactorily degradation efficiency in Acid Red 18, (Sobana and Swaminathan, 2007), Methyl Orange (Xie et al., 2011) and Acridine Orange (Pare et al., 2008).

5. ZnO photocorrosion

The photo-instability and photocorrosion of ZnO in aqueous solution under UV irradiation hinder its usage as an efficient photocatalyst in wastewater treatment. The photocorrosion occurs in 4 steps as follows (Eqs. (37)–(40)) (Gerischer, 1966):

$$O^{2-}_{surface} + h^{+}_{VB} \rightarrow O^{-}_{surface} \quad (37)$$

$$O^{-}_{surface} + 3O^{2-} + 3h^{+}_{VB} \rightarrow 2\left(O - O^{2-}\right) \quad (38)$$

$$\left(O - O^{2-}\right) + 2h^{+}_{VB} \rightarrow O_2 \quad (39)$$

$$2Zn^{2+} \rightarrow 2Zn^{2+}\,(aq) \quad (40)$$

The overall reaction of photocorrosion of ZnO is shown in Eq. (41):

$$ZnO + 2h^{+}_{VB} \rightarrow Zn^{2+} + \tfrac{1}{2}\,O_2 \quad (41)$$

It can be seen that the reaction between the positively holes and the surface oxygen of ZnO is the key factor for the dissolution of ZnO. Moreover, the vacant sites on the ZnO surface also lead to photocorrosion of ZnO (Bai et al., 2013; Chen et al., 2013a). Some studies reported that the photocatalytic activity of ZnO remained after a few cycles (Akyol and Bayramoğlu, 2010; Lee et al., 2015). On the contrary, the photodegradation efficiency reduced significantly under photocorrosion (Li et al., 2010; Xiao, 2012; Chen et al., 2013b). A number of studies have been conducted to overcome photocorrosion of ZnO via surface modification with a layer of polyaniline (Zhang et al., 2009a; Ameen et al., 2011), graphitic carbon (Zhang et al., 2009b), fullerene (Fu et al., 2008), and reduced graphene oxide (Zhang et al., 2013). The formation of a passive layer on the ZnO surface, which is less photo-active suppresses the photo-corrosion rate (Rudd and Breslin, 2000; Comparelli et al., 2005). According to Kislov et al. (2009), the occurrence of ZnO photocorrosion was orientation dependent, with only ZnO (0001)-O suffered strong photocorrosion, while ZnO (0001)-O and ZnO (10-10) exhibited only localized dissolution at defect sites.

6. Conclusion and future work

In summary, modified ZnO seems to be the most promising photocatalyst for high photocatalytic activity under UV/visible/solar irradiation. Many literatures have been concluded that reducing the probability of charge carrier recombination rate is one the most significant factors that determine the photocatalytic activity using the modified ZnO photocatalyst. A number of modification techniques and chemical additives have been developed to minimize the recombination losses of charge carriers and extended the spectral response of ZnO to visible spectrum by applying metal-doping, non-metal doping, RE-doping, co-doping and semiconductor coupling with ZnO. Many researchers have been trying to synthesize not only higher active surface area of ZnO photocatalyst but also sunlight-driven ZnO photocatalyst for effective photocatalytic activity. In this manner, addition of electron donors (hole scavengers) or electron mediators with ZnO can further improve the photocatalytic activity by reacting with positive holes (valence band) irreversibly to prohibit charge-carriers recombination as well as prevent backward reaction (non-metal doping). Continuous efforts have been conducted to achieve the solar-driven ZnO photocatalyst by incorporating electron donors together with ZnO is required (RE-doping, co-doping technique). Besides, small band gap semiconductors can inject electrons to the conduction band of large band gap semiconductors, resulting in efficient charge separation and high photocatalytic efficiency (semiconductor coupling). Thus, the energy levels and charge transfer should be considered carefully when designing such photocatalytic degradation system for organic dye, phenolic compounds, and persistent organic pollutants (POPs).

The industrial application of modified ZnO photocatalyst is anticipated for the future due to its high photocatalytic activity, photostability, and nontoxicity. Nevertheless, further modifications are essential to improve its photocatalytic activity under the direct sunlight irradiation by reducing it band gap energy as well as minimizing the recombination losses. Thus, various potential approaches have been employed to further increase ZnO photocatalyst's efficiency in photocatalytic activity under sunlight irradiation, especially applied in the field of organic dye degradation, phenolic compounds removal, and persistent organic pollutants (POPs) degradation. It was believed that modified ZnO photocatalyst is still permit extensive and in-depth study on the electronic and lattice structure in order to truly understand the effect of different doping/loading with cationic, anionic, small band gap of semiconductor, and elements on ZnO photocatalyst. The modelling work is thus required for better understanding of the photocatalytic oxidation degradation mechanism as well as for designing efficient photoreactor/system for organic dye, phenolic compounds, and persistent organic pollutants (POPs) in our waste water stream. The solid outcomes would be the mechanistic understanding of fundamental science, which may be used in waste pollution management via advanced photocatalytic oxidation reactions in order to create the healthy living environment for our next generations.

Acknowledgements

This research is supported by High Impact Research Chancellory Grant UM.C/625/1/HIR/228 (J55001-73873) from the University of Malaya and e-science fund from MOSTI (06-01-03-SF0949).

References

Abdollahi, Y., Abdullah, A.H., Zainal, Z., Yusof, N.A., 2011. Synthesis and characterization of manganese doped ZnO nanoparticles. Int. J. Basic Appl. Sci. 11 (4), 44–50.

Ahmad, M., Ahmed, E., Hong, Z.L., Jiao, X.L., Abbas, T., Khalid, N.R., 2013a. Enhancement in visible light-responsive photocatalytic activity by embedding Cu-doped ZnO nanoparticles on multi-walled carbon nanotubes. Appl. Surf. Sci.

285 (Part B), 702–712.
Ahmad, M., Ahmed, E., Zhang, Y., Khalid, N.R., Xu, J., Ullah, M., Hong, Z., 2013b. Preparation of highly efficient Al-doped ZnO photocatalyst by combustion synthesis. Curr. Appl. Phys. 13 (4), 697–704.
Ahmad, M., Ahmed, E., Hong, Z.L., Iqbal, Z., Khalid, N.R., Abbas, T., Ahmad, I., 2013c. Structural, optical and photocatalytic properties of hafnium doped zinc oxide nanophotocatalyst. Ceram. Int. 39 (8), 8693–8700.
Akyol, A., Bayramoğlu, M., 2005. Photocatalytic degradation of remazol red F3B using ZnO catalyst. J. Hazard. Mater. 124 (1–3), 241–246.
Akyol, A., Bayramoğlu, M., 2010. Performance comparison of ZnO photocatalyst in various reactor systems. J. Chem. Technol. Biotechnol. 85 (11), 1455–1462.
Ameen, S., Akhtar, M.S., Kim, Y.S., Yang, O.B., Shin, H.S., 2011. An effective nanocomposite of polyaniline and ZnO: preparation, characterizations, and its photocatalytic activity. Colloid Polym. Sci. 289 (4), 415–421.
Anandan, S., Ohashi, N., Miyauchi, M., 2010. ZnO-based visible-light photocatalyst: band-gap engineering and multi-electron reduction by co-catalyst. Appl. Catal. B Environ. 100 (3–4), 502–509.
Assi, N., Mohammadi, A., Manuchehri, Q.S., Walker, R.B., 2015. Synthesis and characterization of ZnO nanoparticle synthesized by a microwave-assisted combustion method and catalytic activity for the removal of ortho-nitrophenol. Desalin. Water Treat. 54 (7), 1939–1948.
Ba-Abbad, M.M., Kadhum, A.A.H., Mohamad, A.B., Takriff, M.S., Sopian, K., 2013. Visible light photocatalytic activity of Fe^{3+}-doped ZnO nanoparticle prepared via sol-gel technique. Chemosphere 91 (11), 1604–1611.
Bai, X., Wang, L., Zong, R., Lv, Y., Sun, Y., Zhu, Y., 2013. Performance enhancement of ZnO photocatalyst via synergic effect of surface oxygen defect and graphene hybridization. Langmuir 29 (9), 3097–3105.
Balachandran, S., Swaminathan, M., 2012. Facile fabrication of heterostructured Bi_2O_3-ZnO photocatalyst and its enhanced photocatalytic activity. J. Phys. Chem. C 116 (50), 26306–26312.
Baruah, S., Dutta, J., 2009. Hydrothermal growth of ZnO nanostructures. Sci. Technol. Adv. Mater. 10 (1), 013001.
Batzill, M., Morales, E.H., Diebold, U., 2006. Influence of nitrogen doping on the defect formation and surface properties of TiO_2 rutile and anatase. Phys. Rev. Lett. 96, 026103.
Bayarri, B., Abellan, M.N., Gimenez, J., Esplugas, S., 2007. Study of the wavelength effect in the photolysis and heterogeneous photocatalysis. Catal. Today 129 (1–2), 231–239.
Behnajady, M.A., Modirshahla, N., Hamzavi, R., 2006. Kinetic study on photocatalytic degradation of C.I. Acid Yellow 23 by ZnO photocatalyst. J. Hazard. Mater. 133 (1–3), 226–232.
Benhebal, H., Chaib, M., Leonard, A., Lambert, S.D., Crine, M., 2012. Photodegradation of phenol and benzoic acid by sol-gel-synthesized alkali metal-doped ZnO. Mater. Sci. Semicond. Process. 15 (3), 264–269.
Chandraboss, V.L., Natanapatham, L., Karthikeyan, B., Kamalakkannan, J., Prabha, S., Senthilvelan, S., 2013. Effect of bismuth doping on the ZnO nanocomposite material and study of its photocatalytic activity under UV-light. Mater. Res. Bull. 48 (10), 3707–3712.
Chatzitakis, A., Berberidou, C., Paspaltsis, I., Kyriakou, G., Sklaviadis, T., Poulios, I., 2008. Photocatalytic degradation and drug activity reduction of chloramphenicol. Water Res. 42 (1–2), 386–394.
Chen, Y., Bagnall, D.M., Koh, H.-J., Park, K.-T., Hiraga, K., Zhu, Z.-Q., Yao, T., 1998. Plasma assisted molecular beam epitaxy of ZnO on *c*-plane sapphire: growth and characterization. J. Appl. Phys. 84 (7), 3912–3918.
Chen, L.-C., Tu, Y.-J., Wang, Y.-S., Kan, R.-S., Huang, C.-M., 2008. Characterization and photoreactivity of N-, S-, and C-doped ZnO under UV and visible light illumination. J. Photochem. Photobiol. A Chem. 199 (2–3), 170–178.
Chen, T.-T., Chang, I.-C., Yang, M.-H., Chiu, H.-T., Lee, C.-Y., 2013a. The exceptional photo-catalytic activity of ZnO/RGO composite via metal and oxygen vacancies. Appl. Catal. B Environ. 142–143, 442–449.
Chen, Z., Zhang, N., Xu, Y.J., 2013b. Synthesis of graphene-ZnO nanorod nanocomposites with improved photoactivity and anti-photocorrosion. CrystEngComm 15, 3022–3030.
Chong, M.N., Jin, B., Chow, C.W.K., Saint, C., 2010. Recent developments in photocatalytic water treatment technology: a review. Water Res. 44 (10), 2997–3027.
Chu, F.-H., Huang, C.-W., Hsin, C.-L., Wang, C.-W., Yu, S.-Y., Yeh, P.-H., Wu, W.-W., 2012. Well-aligned ZnO nanowires with excellent field emission and photocatalytic properties. Nanoscale 4 (5), 1471–1475.
Coleman, V.A., Bradby, J.E., Jagadish, C., 2005. Mechanical properties of ZnO epitaxial layers grown on *a*- and *c*-axis sapphire. Appl. Phys. Lett. 86 (20), 203105.
Comparelli, R., Fanizza, E., Curri, M.L., Cozzoli, P.D., Mascolo, G., Agostiano, A., 2005. UV-induced photocatalytic degradation of azo dyes by organic-capped ZnO nanocrystals immobilized onto substrates. Appl. Catal. B Environ. 60 (1–2), 1–11.
Dai, K., Lu, L., Liang, C., Dai, J., Zhu, G., Liu, Z., Liu, Q., Zhang, Y., 2014. Graphene oxide modified ZnO nanorods hybrid with high reusable photocatalytic activity under UV-LED irradiation. Mater. Chem. Phys. 143 (3), 1410–1416.
Daneshvar, N., Salari, D., Khataee, A.R., 2004. Photocatalytic degradation of azo dye acid red 14 in water on ZnO as an alternative catalyst to TiO_2. J. Photochem. Photobiol. A Chem. 162 (2–3), 317–322.
Daneshvar, N., Aber, S., Seyed Dorraji, M.S., Khataee, A.R., Rasoulifard, M.H., 2007. Photocatalytic degradation of the insecticide diazinon in the presence of prepared nanocrystalline ZnO powders under irradiation of UV-C light. Sep. Purif. Technol. 58 (1), 91–98.
Danwittayakul, S., Jaisai, M., Dutta, J., 2015. Efficient solar photocatalytic degradation of textile wastewater using ZnO/ZTO composites. Appl. Catal. B Environ. 163, 1–8.
Davis, A., Huang, C., 1989. Removal of phenols from water by a photocatalytic oxidation process. Water Sci. Technol. 21 (6–7), 455–464.
Divband, B., Khatamian, M., Eslamian, G.R.K., Darbandi, M., 2013. Synthesis of Ag/ZnO nanostructures by different methods and investigation of their photocatalytic efficiency for 4-nitrophenol degradation. Appl. Surf. Sci. 284, 80–86.
Dixit, A., Mungray, A.K., Chakraborty, M., 2010. Photochemical oxidation of phenol and chlorophenol by $UV/H_2O_2/TiO_2$ process: a kinetic study. Int. J. Chem. Eng. Appl. 1 (3), 247–250.
Dong, F., Zhao, W., Wu, Z., Guo, S., 2009. Band structure and visible light photocatalytic activity of multi-type nitrogen doped TiO_2 nanoparticles prepared by thermal decomposition. J. Hazard. Mater. 162 (2–3), 763–770.
Dubbaka, S., 2008. Branched Zinc Oxide Nanostructures: Synthesis and Photo Catalysis Study for Application in Dye Sensitized Solar Cells, UMI Microform. ProQuest LLC, USA.
Dutta, R.K., Nenavathu, B.P., Talukdar, S., 2014. Anomalous antibacterial activity and dye degradation by selenium doped ZnO nanoparticles. Colloids Surf. B Biointerfaces 114, 218–224.
Elmolla, E.S., Chaudhuri, M., 2010. Degradation of amoxicillin, ampicillin and cloxacillin antibiotics in aqueous solution by the UV/ZnO photocatalytic process. J. Hazard. Mater. 173 (1–3), 445–449.
Erhart, P., Albe, K., 2006. Diffusion of zinc vacancies and interstitials in zinc oxide. Appl. Phys. Lett. 88, 201918.
Etacheri, V., Roshan, R., Kumar, V., 2012. Mg-doped ZnO nanoparticles for efficient sunlight-driven photocatalysis. ACS Appl. Mater. Interfaces 4 (5), 2717–2725.
Evgenidou, E., Fytianos, K., Poulios, I., 2005a. Semiconductor-sensitized photodegradation of dichlorvos in water using TiO_2 and ZnO as catalysts. Appl. Catal. B Environ. 59 (1–2), 81–89.
Evgenidou, E., Fytianos, K., Poulios, I., 2005b. Photocatalytic oxidation of dimethoate in aqueous solutions. J. Photochem. Photobiol. A Chem. 175, 29–38.
Fang, T.-H., Chang, W.-J., Lin, C.-M., 2007. Nanoindentation characterization of ZnO thin films. Mater. Sci. Eng. A 452–453, 715–720.
Feng, X., Guo, H., Patel, K., Zhou, H., Lou, X., 2014. High performance, recoverable Fe_3O_4-ZnO nanoparticles for enhanced photocatalytic degradation of phenol. Chem. Eng. J. 244, 327–334.
Fu, H.B., Xu, T.G., Zhu, S.B., Zhu, Y.F., 2008. Photocorrosion inhibition and enhancement of photocatalytic activity for ZnO via hybridization with C_{60}. Environ. Sci. Technol. 42, 8064–8069.
Fujishima, A., Zhang, X.T., Tryk, D.A., 2008. TiO_2 photocatalysis and related surface phenomena. Surf. Sci. Rep. 63, 515–582.
Ganesh, I., Sekhar, P.S.C., Padmanabham, G., Sundararajan, G., 2012. Influence of Li-doping on structural characteristics and photocatalytic activity of ZnO nanopowder formed in a novel solution pyro-hydrolysis route. Appl. Surf. Sci. 259, 524–537.
Gaya, U.I., Abdullah, A.H., 2008. Heterogeneous photocatalytic degradation of organic contaminants over titanium dioxide: a review of fundamentals, progress and problems. J. Photochem. Photobiol. C Photochem. Rev. 9 (1), 1–12.
Gaya, U.I., Abdullah, A.H., Zainal, Z., Hussein, M.Z., 2009. Photocatalytic treatment of 4-chlorophenol in aqueous ZnO suspensions: intermediates, influence of dosage and inorganic anions. J. Hazard. Mater 168 (1), 57–63.
Gerischer, H., 1966. Electrochemical behavior of semiconductors under illumination. J. Electrochem. Soc. 113 (11), 1174–1182.
Gomez-Solís, C., Ballesteros, J.C., Torres-Martínez, L.M., Juárez-Ramírez, I., Torres, L.A.D., Zarazua-Morin, M.E., Lee, S.W., 2015. Rapid synthesis of ZnO nano-corncobs from Nital solution and its application in the photodegradation of Methyl Orange. J. Photochem. Photobiol. A Chem. 298, 49–54.
Guo, Y., Wang, H., He, C., Qiu, L., Cao, X., 2009. Uniform carbon-coated ZnO nanorods: microwave-assisted preparation, cytotoxicity, and photocatalytic activity. Langmuir 25, 4678–4684.
Haibo, O., Feng, H.J., Cuiyan, L., Liyun, C., Jie, F., 2014. Synthesis of carbon doped ZnO with a porous structure and its solar-light photocatalytic properties. Mater. Lett. 111, 217–220.
Han, Z., Li, S., Chu, J., Chen, Y., 2013. Electrospun Pd-doped ZnO nanofibers for enhanced photocatalytic degradation of Methylene Blue. J. Sol Gel Sci. Technol. 66 (1), 139–144.
Haque, M.M., Muneer, M., Bahnemann, D.W., 2006. Semiconductor-mediated photocatalyzed degradation of a herbicide derivative, chlorotoluron, in aqueous suspensions. Environ. Sci. Technol. 40 (15), 4765–4770.
Hasnat, M.A., Uddin, M.M., Samed, A.J.F., Alam, S.S., Hossain, S., 2007. Adsorption and photocatalytic decolorization of a synthetic dye erythrosine on anatase TiO_2 and ZnO surfaces. J. Hazard. Mater. 147 (1–2), 471–477.
Hayat, K., Gondal, M.A., Khaled, M.M., Ahmed, S., Shemsi, A.M., 2011. Nano ZnO synthesis by modified sol gel method and its application in heterogeneous photocatalytic removal of phenol from water. Appl. Catal. A General 393 (1–2), 122–129.
Hazime, R., Nguyen, Q.H., Ferronato, C., Salvador, A., Jaber, F., Chovelon, J.-M., 2014. Comparative study of imazalil degradation in three systems: UV/TiO_2, $UV/K_2S_2O_8$ and $UV/TiO_2/K_2S_2O_8$. Appl. Catal. B Environ. 144, 286–291.
He, R., Hocking, R.K., Tsuzuki, T., 2012. Co-doped ZnO nanopowders: location of cobalt and reduction in photocatalytic activity. Mater. Chem. Phys. 132 (2–3), 1035–1040.
Helaïli, N., Bessekhouad, Y., Bouguelia, A., Trari, M., 2010. *P*-Cu_2O/*n*-ZnO heterojunction applied to visible light orange II degradation. Sol. Energy 84 (7),

1187–1192.
Herrmann, J.M., 1999. Heterogeneous photocatalysis: fundamentals and applications to the removal of various types of aqueous pollutants. Catal. Today 53 (1), 115–129.
Hong, R.Y., Zhang, S.Z., Di, G.Q., Li, H.Z., Zheng, Y., Ding, J., Wei, D.G., 2008a. Preparation, characterization and application of Fe_3O_4/ZnO core/shell magnetic nanoparticles. Mater. Res. Bull. 43 (8–9), 2457–2468.
Hong, W.-K., Jo, G., Kwon, S.-S., Song, S., Lee, T., 2008b. Electrical properties of surface-tailored ZnO nanowire field-effect transistors. IEEE Trans. Electron Devices 55 (11), 3020–3029.
Hsu, C.C., Wu, N.L., 2005. Synthesis and photocatalytic activity of ZnO/ZnO_2 composite. J. Photochem. Photobiol. A Chem. 172 (3), 269–274.
Hughes, W.L., Wang, Z.L., 2004. Formation of piezoelectric single-crystal nanorings and nanobows. J. Am. Chem. Soc. 126 (21), 6703–6709.
Hullavarad, S., Hullavarad, N., Look, D., Claflin, B., 2009. Persistent photoconductivity studies in nanostructured ZnO UV sensors. Nanoscale Res. Lett. 4 (12), 1421–1427.
Hwang, D.-K., Oh, M.-S., Lim, J.-H., Park, S.-J., 2007. ZnO thin films and light-emitting diodes. J. Phys. D Appl. Phys. 40 (22), R387–R412.
Irie, H., Watanabe, Y., Hashimoto, K., 2003. Nitrogen-concentration dependence on photocatalytic activity of $TiO_{2-x}N_x$ powders. J. Phys. Chem. B 107 (23), 5483–5486.
Ivetić, T.B., Dimitrievska, M.R., Finčur, N.L., Crossed D Signačanin, L.R., Gúth, I.O., Abramović, B.F., Lukić-Petrović, S.R., 2014. Effect of annealing temperature on structural and optical properties of Mg-doped ZnO nanoparticles and their photocatalytic efficiency in alprazolam degradation. Ceram. Int. 40 (1 Part B), 1545–1552.
Jagadish, C., Pearton, S., 2006. Zinc Oxide Bulk, Thin Films and Nanostructures, first ed. Elsevier Science, Gainesville USA.
Janotti, A., Van de Walle, C.G., 2009. Fundamentals of zinc oxide as a semiconductor. Rep. Prog. Phys. 72 (12), 126501.
Jian, S.-R., Teng, I.-J., Yang, P.-F., Lai, Y.-S., Lu, J.-M., Chang, J.-G., Ju, S.-P., 2008. Surface Morphological and nanomechanical properties of PLD-derived ZnO thin films. Nanoscale Res. Lett. 3 (5), 186–193.
Jiang, J., Zhang, X., Sun, P., Zhang, L., 2011. ZnO-BiOI heterostructures-photoinduced charge-transfer property and enhanced visible-light photocatalytic activity. J. Phys. Chem. C 115 (42), 20555–20564.
Karunakaran, C., Rajeswari, V., Gomathisankar, P., 2011. Combustion synthesis of ZnO and Ag-doped ZnO and their bactericidal and photocatalytic activities. Superlattices Microstruct. 50 (3), 234–241.
Kato, S., Hirano, Y., Iwata, M., Sano, T., Takeuchi, K., Matsuzawa, S., 2005. Photocatalytic degradation of gaseous sulphur compounds by silver-deposited titanium dioxide. Appl. Catal. B Environ. 57 (2), 109–115.
Khattab, I.A., Ghaly, M.Y., Sterlund, L.O., Ali, M.E.M., Farah, J.Y., Zaher, F.M., Badawy, M.I., 2012. Photocatalytic degradation of azo dye reactive red 15 over synthesized titanium and zinc oxides photocatalysts: a comparative study. Desalin. Water Treat. 48 (1–3), 120–129.
Khodja, A.A., Sehili, T., Pilichowski, J., Boule, P., 2001. Photocatalytic degradation of 2-phenylphenol on TiO_2 and ZnO in aqueous suspensions. J. Photochem. Photobiol. A Chem. 141, 231–239.
Kim, K.J., Kreider, P.B., Choi, C., Chang, C.H., Ahn, H.G., 2013. Visible-light-sensitive Na-doped p-type flower-like ZnO photocatalysts synthesized via a continuous flow microreactor. RSC Adv. 3 (31), 12702–12710.
King, D.S., Nix, R.M., 1996. Thermal stability and reducibility of ZnO and Cu/ZnO catalysts. J. Catal. 160, 76–83.
Kislov, N., Lahiri, J., Verma, H., Goswami, D.Y., Stefanakos, E., Batzill, M., 2009. Photocatalytic degradation of Methyl Orange over single crystalline ZnO: orientation dependence of photoactivity and photostability of ZnO. Langmuir 25 (5), 3310–3315.
Kong, X.Y., Wang, Z.L., 2003. Spontaneous polarization-induced nanohelixes, nanosprings, and nanorings of piezoelectric nanobelts. Nano Lett. 3 (12), 1625–1631.
Kositzi, M., Poulios, I., Samara, K., Tsatsaroni, E., Darakas, E., 2007. Photocatalytic oxidation of Cibacron Yellow LS-R. J. Hazard. Mater. 146 (3), 680–685.
Kosmulski, M., 2006. pH-dependent surface charging and points of zero charge III. Update. J. Colloid Interface Sci. 298 (2), 730–741.
Krishnakumar, B., Selvam, K., Velmurugan, R., Swaminathan, M., 2010. Influence of operational parameters on photodegradation of Acid Black 1 with ZnO. Desalin. Water Treat. 24 (1–3), 132–139.
Kucheyev, S.O., Bradby, J.E., Williams, J.S., Jagadish, C., 2002. Mechanical deformation of single-crystal ZnO. Appl. Phys. Lett. 80 (6), 956–958.
Kudo, A., Miseki, Y., 2009. Heterogeneous photocatalyst materials for water splitting. Chem. Soc. Rev. 38, 253–278.
Kumar, S., Sahare, P.D., 2012. Nd-doped ZnO as a multifunctional nanomaterial. J. Rare Earths 30 (8), 761–768.
Kumar, S., Sahare, P.D., 2014b. Gd^{3+} incorporated ZnO nanoparticles: a versatile material. Mater. Res. Bull. 51, 217–223.
Kumar, K., Chitkara, M., Sandhu, I.S., Mehta, D., Kumar, S., 2014a. Photocatalytic, optical and magnetic properties of Fe-doped ZnO nanoparticles prepared by chemical route. J. Alloys Compd. 588, 681–689.
Kurbanov, S., Yang, W.C., Kang, T.W., 2011. Kelvin probe force microscopy of defects in ZnO nanocrystals associated with emission at 3.31 eV. Appl. Phys. Express 4 (2), 021101.
Kuzhalosai, V., Subash, B., Senthilraja, A., Dhatshanamurthi, P., Shanthi, M., 2013. Synthesis, characterization and photocatalytic properties of SnO_2-ZnO composite under UV-A light. Spectrochim. Acta Part A Mol. Biomol. Spectrosc. 115, 876–882.
Lai, Y., Meng, M., Yu, Y., 2010. One-step synthesis, characterizations and mechanistic study of nanosheets-constructed fluffy ZnO and Ag/ZnO spheres used for Rhodamine B photodegradation. Appl. Catal. B Environ. 100 (3–4), 491–501.
Lai, Y., Meng, M., Yu, Y., Wang, X., Ding, T., 2011. Photoluminescence and photocatalysis of the flower-like nano-ZnO photocatalysts prepared by a facile hydrothermal method with or without ultrasonic assistance. Appl. Catal. B Environ. 105 (3–4), 335–345.
Lam, S.-M., Sin, J.-C., Abdullah, A.Z., Mohamed, A.R., 2013a. ZnO nanorods surface-decorated by WO_3 nanoparticles for photocatalytic degradation of endocrine disruptors under a compact fluorescent lamp. Ceram. Int. 39 (3), 2343–2352.
Lam, S.-M., Sin, J.-C., Abdullah, A.Z., Mohamed, A.R., 2013b. Efficient photodegradation of endocrine-disrupting chemicals with Bi_2O_3-ZnO nanorods under a compact fluorescent lamp. Water Soil Air Pollut. 224, 1565.
Lam, S.-M., Sin, J.-C., Abdullah, A.Z., Mohamed, A.R., 2013c. Investigation on visible-light photocatalytic degradation of 2,4-dichlorophenoxyacetic acid in the presence of MoO_3/ZnO nanorod composites. J. Mol. Catal. A Chem. 370, 123–131.
Lam, S.-M., Sin, J.-C., Satoshi, I., Abdullah, A.Z., Mohamed, A.R., 2014. Enhanced sunlight photocatalytic performance over Nb_2O_5/ZnO nanorod composites and the mechanism study. Appl. Catal. A General 471, 126–135.
Lee, K.M., Hamid, S.B.A., Lai, C.W., 2015. Multivariate analysis of photocatalytic-mineralization of Eriochrome Black T dye using ZnO catalyst and UV irradiation. Mater. Sci. Semicond. Process. 39, 40–48.
Lewis, N.S., 2007. Toward cost-effective solar energy use. Science 315, 798–801.
Li, H., Liang, C., Zhong, K., Liu, M., Hope, G.A., Tong, Y., Liu, P., 2009. The modulation of optical property and its correlation with microstructures of ZnO nanowires. Nanoscale Res. Lett. 4, 1183–1190.
Li, B., Wang, Y., 2010. Facile synthesis and photocatalytic activity of ZnO-CuO nanocomposite. Superlattices Microstruct 47, 615–623.
Li, Y., Xie, W., Hu, X., Shen, G., Zhou, X., Xiang, Y., Zhao, X., Fang, P., 2010. Comparison of dye photodegradation and its coupling with light-to-electricity conversion over TiO2 and ZnO. Langmuir 26 (1), 591–597.
Li, B., Wang, Y., 2011a. Synthesis, microstructure, and photocatalysis of ZnO/CdS nano-heterostructure. J. Phys. Chem. Solids 72 (10), 1165–1169.
Li, C., Chen, R., Zhang, X., Shu, S., Xiong, J., Zheng, Y., Dong, W., 2011b. Electrospinning of CeO_2-ZnO composite nanofibers and their photocatalytic property. Mater. Lett. 65 (9), 1327–1330.
Li, B., Liu, T., Wang, Y., Wang, Z., 2012a. ZnO/graphene-oxide nanocomposite with remarkably enhanced visible-light-driven photocatalytic performance. J. Colloid Interface Sci. 377 (1), 114–121.
Li, M., Xing, G., Ah Qune, L.F.N., Xing, G., Wu, T., Huan, C.H.A., Zhang, X., Sum, T.C., 2012b. Tailoring the charge carrier dynamics in ZnO nanowires: the role of surface hole/electron traps. Phys. Chem. Chem. Phys. 14, 3075–3082.
Li, J.Z., Zhong, J.B., Hu, W., Lu, Y., Zeng, J., Shen, Y.C., 2013. Fabrication of tin-doped zinc oxide by parallel flow co-precipitation with enhanced photocatalytic performance. Mater. Sci. Semicond. Process. 16 (1), 143–148.
Li, D., Huang, J.-F., Cao, L.-Y., Li, J.-Y., OuYang, H.-B., Yao, C.-Y., 2014a. Microwave hydrothermal synthesis of Sr^{2+} doped ZnO crystallites with enhanced photocatalytic properties. Ceram. Int. 40 (2), 2647–2653.
Li, D., Huang, J.-F., Cao, L.-Y., Ou, H.-B., Yao, C.-Y., 2014b. Microwave hydrothermal synthesis of K^+ doped ZnO nanoparticles with enhanced photocatalytic properties under visible-light. Mater. Lett. 118, 17–20.
Li, Y., Wang, Y., Liu, L., Wang, D., Zhang, W., 2014c. Ag/ZnO hollow sphere composites: reusable photocatalyst for photocatalytic degradation of 17α-ethinylestradiol. Environ. Sci. Pollut. Res. 21 (7), 5177–5186.
Liao, W., Zheng, T., Wang, P., Tu, S., Pan, W., 2010. Efficient microwave-assisted photocatalytic degradation of endocrine disruptor dimethyl phthalate over composite catalyst ZrO_x/ZnO. J. Environ. Sci. 22 (11), 1800–1806.
Liu, Z.-L., Deng, J.-C., Deng, J.-J., Li, F.-F., 2008. Fabrication and photocatalysis of CuO/ZnO nano-composites via a new method. Mater. Sci. Eng. B 150 (2), 99–104.
Liu, Y., Kang, Z.H., Chen, Z.H., Shafiq, I., Zapien, J.A., Bello, I., Zhang, W.J., Lee, S.T., 2009. Synthesis, characterization, and photocatalytic application of different ZnO nanostructures in array configurations. Cryst. Growth Des. 9, 3222–3227.
Liu, K., Sakurai, M., Aono, M., 2010. ZnO-based ultraviolet photodetectors. Sensors 10 (9), 8604–8634.
Liu, I.-T., Hon, M.H., Teoh, L.G., 2014. The preparation, characterization and photocatalytic activity of radical-shaped CeO_2-ZnO microstructures. Ceram. Int. 40, 4019–4024.
Look, D.C., 2001. Recent advances in ZnO materials and devices. Mater. Sci. Eng. B 80 (1–3), 383–387.
Lu, J.G., Ye, Z.Z., Huang, J.Y., Zhu, L.P., Zhao, B.H., 2006. ZnO quantum dots synthesized by a vapor phase transport process. Appl. Phys. Lett. 88, 063110.
Lu, C., Wu, Y., Mai, F., Chung, W., Wu, C., Lin, W., Chen, C., 2009. Degradation efficiencies and mechanisms of the ZnO-mediated photocatalytic degradation of Basic Blue 11 under visible light irradiation. J. Mol. Catal. A Chem. 310 (1–2), 159–165.
Maggard, P.A., Stern, C.L., Poeppelmeier, K.R., 2001. Understanding the role of helical chains in the formation of noncentrosymmetric solids. J. Am. Chem. Soc. 123 (31), 7742–7743.
Mahalakshmi, M., Arabindoo, B., Palanichamy, M., Murugesan, V., 2007. Photocatalytic degradation of carbofuran using semiconductor oxides. J. Hazard. Mater. 143 (1–2), 240–245.
Mai, F.D., Chen, C.C., Chen, J.L., Liu, S.C., 2008. Photodegradation of Methyl Green

using visible irradiation in ZnO suspensions: Determination of the reaction pathway and identification of intermediates by a high-performance liquid chromatography–photodiode array-electrospray ionization-mass spectrometry method. J. Chromatogr. A 1189 (1–2), 355–365.
Maiti, U.N., Maiti, S., Chattopadhyay, K.K., 2012. An ambient condition, one pot route for large scale production of ultrafine (<15 nm) ZnO nanowires from commercial zinc exhibiting excellent recyclable catalytic performance: approach extendable to CuO nanostructures. CrystEngComm 14, 640–647.
Malato, S., Blanco, J., Campos, A., Caceres, J., Guillard, C., Herrmann, J.M., Fernandez-Alba, A.R., 2003. Effect of operating parameters on the testing of new industrial titania catalysts at solar pilot plant scale. Appl. Catal. B Environ. 42 (4), 349–357.
Malato, S., Fernandez-Ibanez, P., Maldonado, M.I., Blanco, J., Gernjak, W., 2009. Decontamination and disinfection of water by solar photocatalysis: recent overview and trends. Catal. Today 147 (1), 1–59.
Mijin, D., Savić, M., Snežana, P., Smiljanić, A., Glavaški, O., Jovanović, M., Petrović, S., 2009. A study of the photocatalytic degradation of metamitron in ZnO water suspensions. Desalination 249 (1), 286–292.
Mills, A., Hunte, S.L., 1997. An overview of semiconductor photocatalysis. J. Photochem. Photobiol. A Chem. 108 (1), 1–35.
Mohan, R., Krishnamoorthy, K., Kim, S.-J., 2012. Enhanced photocatalytic activity of Cu-doped ZnO nanorods. Solid State Commun. 152 (5), 375–380.
Moore, D., Wang, Z.L., 2006. Growth of anisotropic one-dimensional ZnS nanostructures. J. Mater. Chem. 16 (40), 3898–3905.
Morkoç, H., Özgür, Ü., 2009. Zinc Oxide: Fundamentals, Materials and Device Technology, first ed. Wiley-VCH, UK.
Mrowetz, M., Selli, E., 2006. Photocatalytic degradation of formic and benzoic acids and hydrogen peroxide evolution in TiO_2 and ZnO water suspensions. J. Photochem. Photobiol. A Chem. 180 (1–2), 15–22.
Nagaveni, K., Hegde, M.S., Ravishankar, N., Subbanna, G.N., Madras, G., 2004. Synthesis and structure of nanocrystalline TiO_2 with lower band gap showing high photocatalytic activity. Langmuir 20 (7), 2900–2907.
Nenavathu, B.P., Krishna Rao, A.V.R., Goyal, A., Kapoor, A., Dutta, R.K., 2013. Synthesis, characterization and enhanced photocatalytic degradation efficiency of Se doped ZnO nanoparticles using trypan blue as a model dye. Appl. Catal. A General 459, 106–113.
Nezamzadeh-Ejhieh, A., Khodabakhshi-Chermahini, F., 2014. Incorporated ZnO onto nano clinoptilolite particles as the active centers in the photodegradation of phenylhydrazine. J. Ind. Eng. Chem. 20 (2), 695–704.
Nickel, N.H., Terukov, E., 2005. Zinc Oxide-A Material for Micro- and Optoelectronic Applications. Springer Netherlands. Springer Science+Business Media B.V.
Ochuma, I.J., Fishwick, R.P., Wood, J., Winterbottom, J.M., 2007. Optimisation of degradation conditions of 1,8-diazabicyclo[5.4.0]undec-7-ene in water and reaction kinetics analysis using a cocurrent downflow contactor photocatalytic reactor. Appl. Catal. B Environ 73 (3–4), 259–268.
Ogale, S.B., 2005. Thin Films and Heterostructures for Oxide Electronics. Springer (Springer-Verlac US).
Omidi, A., Habibi-Yangjeh, A., Pirhashemi, M., 2013. Application of ultrasonic irradiation method for preparation of ZnO nanostructures doped with Sb^{+3} ions as a highly efficient photocatalyst. Appl. Surf. Sci. 276, 468–475.
Özgür, Ü., Alivov, Y.I., Liu, C., Teke, A., Reshchikov, M.A., Do ğan, S., Avrutin, V., Cho, S.-J., Morkoç, H., 2005. A comprehensive review of ZnO materials and devices. J. Appl. Phys. 98 (4), 041301.
Palominos, R.A., Mondaca, M.A., Giraldo, A., Peñuela, G., Pérez-Moya, M., Mansilla, H.D., 2009. Photocatalytic oxidation of the antibiotic tetracycline on TiO_2 and ZnO suspensions. Catal. Today 144 (1–2), 100–105.
Pant, H.R., Park, C.H., Pant, B., Tijing, L.D., Kim, H.Y., Kim, C.S., 2012. Synthesis, characterization, and photocatalytic properties of ZnO nano-flower containing TiO_2 NPs. Ceram. Int. 38 (4), 2943–2950.
Pare, B., Jonnalagadda, S.B., Tomar, H., Singh, P., Bhagwat, V.W., 2008. ZnO assisted photocatalytic degradation of acridine orange in aqueous solution using visible irradiation. Desalination 232 (1–3), 80–90.
Patil, A.B., Patil, K.R., Pardeshi, S.K., 2010. Ecofriendly synthesis and solar photocatalytic activity of S-doped ZnO. J. Hazard. Mater. 183 (1–3), 315–323.
Peng, W.Q., Qu, S.C., Cong, G.W., Wang, Z.G., 2006. Synthesis and temperature-dependent near-band-edge emission of chain-like Mg-doped ZnO nanoparticles. Appl. Phys. Lett. 88 (10), 101902.
Peng, L.L., Xie, T.F., Lu, Y.C., Fan, H.M., Wang, D.J., 2010. Synthesis, photoelectric properties and photocatalytic activity of the Fe_2O_3/TiO_2 heterogeneous photocatalysts. Phys. Chem. Chem. Phys. 12, 8033–8041.
Peternel, I.T., Koprivanac, N., Božić, A.M.L., Kušić, H.M., 2007. Comparative study of UV/TiO_2, UV/ZnO and photo-fenton processes for the organic reactive dye degradation in aqueous solution. J. Hazard. Mater. 148 (1–2), 477–484.
Phuruangrat, A., Kongpet, W., Yayapao, O., Kuntalue, B., Thongtem, S., Thongtem, T., 2014a. Ultrasonic-assisted synthesis, characterization, and optical properties of Sb doped ZnO and their photocatalytic activities. J. Nanomater 2014, 10. Article ID 725817.
Phuruangrat, A., Yayapao, O., Thongtem, T., Thongtem, S., 2014b. Synthesis and characterization of europium-doped zinc oxide photocatalyst. J. Nanomater. 2014, 9. Article ID 367529.
Phuruangrat, A., Yayapao, O., Thongtem, T., Thongtem, S., 2014c. Preparation, characterization and photocatalytic properties of Ho doped ZnO nanostructures synthesized by sonochemical method. Superlattices Microstruct. 67, 118–126.
Porter, F.C., 1991. Zinc Handbook: Properties, Processing and Use in Design, first ed. Marcel Dekker, New York USA.
Pozan, G.S., Kambur, A., 2014. Significant enhancement of photocatalytic activity over bifunctional ZnO-TiO_2 catalysts for 4-chlorophenol degradation. Chemosphere 105, 152–159.
Qiu, Y., Yang, M., Fan, H., Xu, Y., Shao, Y., Yang, X., Yang, S., 2013. Synthesis and characterization of nitrogen doped ZnO tetrapods and application in photocatalytic degradation of organic pollutants under visible light. Mater. Lett. 99, 105–107.
Rabindranathan, S., Devipriya, S., Yesodharan, S., 2003. Photocatalytic degradation of phosphamidon on semiconductor oxides. J. Hazard. Mater. 102 (2–3), 217–229.
Reynolds, D.C., Look, D.C., Jogai, B., 1996. Optically pumped ultraviolet lasing from ZnO. Solid State Commun. 99 (12), 873–875.
Reynolds, D.C., Look, D.C., Jogai, B., Litton, C.W., Cantwell, G., Harsch, W.C., 1999. Valence-band ordering in ZnO. Phys. Rev. B 60 (4), 2340–2344.
Rincon, A.G., Pulgarin, C., 2005. Use of coaxial photocatalytic reactor (CAPHORE) in the TiO_2 photo-assisted treatment of mixed E. coli and Bacillus sp. and bacterial community present in wastewater. Catal. Today 101 (3–4), 331–344.
Rodnyi, P.A., Khodyuk, I.V., 2011. Optical and luminescence properties of zinc oxide. Opt. Spectrosc. 111 (5), 776–785.
Rudd, A.L., Breslin, C.B., 2000. Photo-induced dissolution of zinc in alkaline solutions. Electrochimica Acta 45 (10), 1571–1579.
Sakthivel, S., Geissen, S.U., Bahnemann, D.W., Murugesan, V., Vogelpohl, A., 2002. Enhancement of photocatalytic activity by semiconductor heterojunctions: α-Fe_2O_3, WO_3 and CdS deposited on ZnO. J. Photochem. Photobiol. A Chem. 148 (1–3), 283–293.
Saleh, R., Djaja, N.F., 2014. Transition-metal-doped ZnO nanoparticles: synthesis, characterization and photocatalytic activity under UV light. Spectrochim. Acta Part A Mol. Biomol. Spectrosc. 130, 581–590.
Samadi, M., Shivaee, H.A., Pourjavadi, A., Moshfegh, A.Z., 2013. Synergism of oxygen vacancy and carbonaceous species on enhanced photocatalytic activity of electrospun ZnO-carbon nanofibers: charge carrier scavengers mechanism. Appl. Catal. A General 466, 153–160.
Samadi, M., Pourjavadi, A., Moshfegh, A.Z., 2014. Role of CdO addition on the growth and photocatalytic activity of electrospun ZnO nanofibers- UV vs. visible light. Appl. Surf. Sci. 298, 147–154.
Sanchez, E., Lopez, T., 1995. Effect of the preparation method on the bandgap of titania and platinum-titania sol-gel materials. Mater. Lett. 25, 271–275.
Saravanan, R., Shankar, H., Prakash, T., Narayanan, V., Stephen, A., 2011. ZnO/CdO composite nanorods for photocatalytic degradation of Methylene Blue under visible light. Mater. Chem. Phys. 125 (1–2), 277–280.
Sathishkumah, P., Sweena, R., Wu, J.J., Anandan, S., 2011. Synthesis of CuO-ZnO nanophotocatalyst for visible light assisted degradation of a textile dye in aqueous solution. Chem. Eng. J. 171, 136–140.
Schmidt-Mende, L., MacManus-Driscoll, J.L., 2007. ZnO-nanostructures, defects, and devices. Mater. Today 10 (5), 40–48.
Selvam, K., Muruganandham, M., Muthuvel, I., Swaminathan, M., 2007. The influence of inorganic oxidants and metal ions on semiconductor sensitized photodegradation of 4-fluorophenol. Chem. Eng. J. 128 (1), 51–57.
Senthilraja, A., Subash, B., Krishnakumar, B., Rajamanickam, D., Swaminathan, M., Shanthi, M., 2014. Synthesis, characterization and catalytic activity of co-doped Ag-Au-ZnO for MB dye degradation under UV-A light. Mater. Sci. Semicond. Process. 22, 83–91.
Serpone, N., Pelizzetti, E., 1989. Photocatalysis: Fundamentals and Applications, first ed. Wiley-Interscience, John Wiley and Sons, Inc, New York USA.
Serpone, N., Maruthamuthu, P., Pichat, P., Pelizzetti, E., Hidaka, H., 1995. Exploiting the interparticle electron transfer process in the photocatalysed oxidation of phenol, 2-chlorophenol and pentachlorophenol: chemical evidence for electron and hole transfer between coupled semiconductors. J. Photochem. Photobiol. A Chem. 85 (3), 247–255.
Seyed-dorraji, M.S., Daneshvar, N., Aber, S., 2009. Influence of inorganic oxidants and metal ions on photocatalytic activity of prepared zinc oxide nanocrystals. Glob. Nest J. 11 (4), 535–545.
Shafaei, A., Nikazar, M., Arami, M., 2010. Photocatalytic degradation of terephthalic acid using titania and zinc oxide photocatalysts: comparative study. Desalination 252 (1-3), 8–16.
Shang, M., Wang, W.Z., Zhang, L., Sun, S.M., Wang, L., Zhou, L., 2009. 3D Bi_2WO_6/TiO_2 hierarchical heterostructure: controllable synthesis and enhanced visible photocatalytic degradation performances. J. Phys. Chem. C 113 (33), 14727–14731.
Shanthi, M., Kuzhalosai, V., 2012. Photocatalytic degradation of an azo dye, Acid Red 27, in aqueous solution using nano ZnO. Indian J. Chem. 51 (3), 428–434.
Sharmaa, B.K., Khare, N., Haranath, D., 2010. Photoluminescence lifetime of Al-doped ZnO films in visible region. Solid State Commun. 150 (47–48), 2341–2345.
Sherly, E.D., Vijaya, J.J., Selvam, N.C.S., Kennedy, L.J., 2014. Microwave assisted combustion synthesis of coupled ZnO-ZrO_2 nanoparticles and their role in the photocatalytic degradation of 2,4-dichlorophenol. Ceram. Int. 40 (4), 5681–5691.
Shifu, C., Gengyu, C., 2005. Photocatalytic degradation of organophosphorus pesticides using floating photocatalyst $TiO_2 \cdot SiO_2$/beads by sunlight. Sol. Energy 79 (1), 1–9.
Shrama, S.K., Saurakhiya, N., Barthwal, S., Kumar, R., Sharma, A., 2014. Tuning of structural, optical, and magnetic properties of ultrathin and thin ZnO nanowire arrays for nano device applications. Nanoscale Res. Lett. 9 (1), 122.
Sin, J.-C., Lam, S.-M., Lee, K.-T., Mohamed, A.R., 2013. Photocatalytic performance of novel samarium-doped spherical-like ZnO hierarchical nanostructures under

visible light irradiation for 2,4-dichlorophenol degradation. J. Colloid Interface Sci. 401, 40–49.
Sin, J.-C., Lam, S.-M., Lee, K.-T., Mohamed, A.R., 2014a. Preparation of rare earth-doped ZnO hierarchical micro/nanospheres and their enhanced photocatalytic activity under visible light irradiation. Ceram. Int. 40 (4), 5431–5440.
Sin, J.-C., Lam, S.-M., Satoshi, I., Lee, K.-T., Mohamed, A.R., 2014b. Sunlight photocatalytic activity enhancement and mechanism of novel europium-doped ZnO hierarchical micro/nanospheres for degradation of phenol. Appl. Catal. B Environ. 148–149, 258–268.
Singh, H.K., Saquib, M., Haque, M.M., Muneer, M., 2007. Heterogeneous photocatalysed degradation of 4-chlorophenoxyacetic acid in aqueous suspensions. J. Hazard. Mater. 142 (1–2), 374–380.
Sirtori, C., Altvater, P.K., Freitas, A.M.D., Peralta-Zamora, P.G., 2006. Degradation of aqueous solutions of camphor by heterogeneous photocatalysis. J. Hazard. Mater. 129 (1–3), 110–115.
Siuleiman, S., Kaneva, N., Bojinovaa, A., Papazova, K., Apostolov, A., Dimitrov, D., 2014. Photodegradation of Orange II by ZnO and TiO_2 powders and nanowire ZnO and ZnO/TiO_2 thin films. Colloids Surfaces A Physicochem. Eng. Aspects 460, 408–413.
Sobana, N., Swaminathan, M., 2007. The effect of operational parameters on the photocatalytic degradation of Acid Red 18 by ZnO. Sep. Purif. Technol. 56 (1), 101–107.
Subash, B., Krishnakumar, B., Velmurugan, R., Swaminathan, M., Shanthi, M., 2012. Synthesis of Ce co-doped Ag-ZnO photocatalyst with excellent performance for NBB dye degradation under natural sunlight illumination. Catal. Sci. Technol. 2 (11), 2319–2326.
Subash, B., Krishnakumar, B., Swaminathan, M., Shanthi, M., 2013a. Highly efficient, solar active, and reusable photocatalyst: Zr-loaded Ag-ZnO for reactive red 120 dye degradation with synergistic effect and dye-sensitized mechanism. Langmuir 29 (3), 939–949.
Subash, B., Krishnakumar, B., Swaminathan, M., Shanthi, M., 2013b. Highly active Zr co-doped Ag-ZnO photocatalyst for the mineralization of Acid Black 1 under UV-A light illumination. Mater. Chem. Phys. 141 (1), 114–120.
Sun, X.W., Liu, Z.J., Chen, Q.C., Lu, W.H., Song, T., Wang, C.W., 2006. Heat capacity of ZnO with cubic structure at high temperatures. Solid State Commun. 140 (5), 219–224.
Sun, S., Chang, X., Li, X., Li, Z., 2013. Synthesis of N-doped ZnO nanoparticles with improved photocatalytical activity. Ceram. Int. 39 (5), 5197–5203.
Suwanboon, S., Amornpitoksuk, P., Bangrak, P., Muensit, N., 2013. Optical, photocatalytic and bactericidal properties of $Zn_{1-x}La_xO$ and $Zn_{1-x}Mg_xO$ nanostructures prepared by a sol-gel method. Ceram. Int. 39 (5), 5597–5608.
Tan, S.T., Chen, B.J., Sun, X.W., Fan, W.J., 2005. Blueshift of optical band gap in ZnO thin films grown by metal-organic chemical-vapor deposition. J. Appl. Phys. 98 (1), 013505.
Uddin, M.T., Nicolas, Y., Olivier, C., Toupance, T., Servant, L., Müller, M.M., Kleebe, H.J., Ziegler, J., Jaegermann, W., 2012. Nanostructured SnO_2-ZnO heterojunction photocatalysts showing enhanced photocatalytic activity for the degradation of organic dyes. Inorg. Chem. 51 (14), 7764–7773.
Umar, A., 2009. Growth of Comb-like ZnO nanostructures for dye-sensitized solar cells applications. Nanoscale Res. Lett. 4 (9), 1004–1008.
Venkatachalam, N., Palanichamy, M., Murugesan, V., 2007. Sol-gel preparation and characterization of alkaline earth metal doped nano TiO_2: efficient photocatalytic degradation of 4-chlorophenol. J. Mol. Catal. A Chem. 273 (1–2), 177–185.
Vignesh, K., Rajarajan, M., Suganthi, A., 2014. Visible light assisted photocatalytic performance of Ni and Th co-doped ZnO nanoparticles for the degradation of Methylene Blue dye. J. Ind. Eng. Chem. 20 (5), 3826–3833.
Vinu, R., Madras, G., 2010. Environmental remediation by photocatalysis. J. Indian Inst. Sci. 90, 189–229.
Wang, Z.L., 2004. Zinc oxide nanostructures: growth, properties and applications. J. Phys. Condens. Matter 16 (25), R829–R858.
Wang, H.Q., Wang, G.Z., Jia, L.C., Tang, C.J., Li, G.H., 2007. Polychromatic visible photoluminescence in porous ZnO nanotubes. J. Phys. D Appl. Phys. 40 (21), 6549–6553.
Wang, J., Tafen, D.N., Lewis, J.P., Hong, Z., Manivannan, A., Zhi, M., Li, M., Wu, N., 2009a. Origin of photocatalytic activity of nitrogen-doped TiO_2 nanobelts. J. Am. Soc. 131 (34), 12290–12297.
Wang, X.W., Liu, G., Chen, Z.G., Li, F., Wang, L.Z., Lu, G.Q., Cheng, H.M., 2009b. Enhanced photocatalytic hydrogen evolution by prolonging the lifetime of carriers in ZnO/CdS heterostructures. Chem. Commun. 3452–3454.
Wei, L., Shifu, C., Wei, Z., Sujuan, Z., 2009. Titanium dioxide mediated photocatalytic degradation of methamidophos in aqueous phase. J. Hazard. Mater. 164 (1), 154–160.
Wu, W., Gao, S., Tu, W., Chen, J., Zhang, P., 2010. Intensified photocatalytic degradation of nitrobenzene by pickering emulsion of ZnO nanoparticles. Particuology 8 (5), 453–457.
Wu, C., Shen, L., Yu, H., Zhang, Y.-C., Huang, Q., 2012. Solvothermal synthesis of Cu-doped ZnO nanowires with visible light-driven photocatalytic activity. Mater. Lett. 74, 236–238.
Wu, C., Zhang, Y.C., Huang, Q., 2013. Solvothermal synthesis of N-doped ZnO microcrystals from commercial ZnO powder with visible light-driven photocatalytic activity. Mater. Lett. 119, 104–106.
Xia, J., Wang, A., Liu, X., Su, Z., 2011. Preparation and characterization of bifunctional, Fe_3O_4/ZnO nanocomposites and their use as photocatalysts. Appl. Surf. Sci. 257 (23), 9724–9732.
Xiao, F.X., 2012. Construction of highly ordered ZnO–TiO_2 nanotube arrays (ZnO/TNTs) heterostructure for photocatalytic application. ACS Appl. Mater. Interfaces 4 (12), 7055–7063.
Xiaoliang, W., Shihua, D., Yong, P., Qin, X., Yun, L., 2013. Study of the photocatalytic activity of Na and Al-doped ZnO powders. Ferroelectrics 455 (1), 90–96.
Xie, J., Li, Y., Zhao, W., Bian, L., Wei, Y., 2011. Simple fabrication and photocatalytic activity of ZnO particles with different morphologies. Powder Technol. 207 (1–3), 140–144.
Xu, C., Cao, L., Su, G., Liu, W., Liu, H., Yu, Y., Qu, X., 2010. Preparation of ZnO/Cu_2O compound photocatalyst and application in treating organic dyes. J. Hazard. Mater. 176 (1–3), 807–813.
Xu, H., Liu, C., Li, H., Xu, Y., Xia, J., Yin, S., Liu, L., Wu, X., 2011. Synthesis, characterization and photocatalytic activity of $NaNbO_3$/ZnO heterojunction photocatalysts. J. Alloys Compd. 509 (37), 9157–9163.
Yang, Z., Lv, L., Dai, Y., Xv, Z., Qian, D., 2010. Synthesis of ZnO-SnO_2 composite oxides by CTAB-assisted co-precipitation and photocatalytic properties. Appl. Surf. Sci. 256 (9), 2898–2902.
Yang, Y., Xu, L., Su, C., Che, J., Sun, W., Gao, H., 2014. Electrospun ZnO-Bi_2O_3 nanofibers with enhanced photocatalytic activity. J. Nanomater. 2014, 7. Article ID: 130539.
Yayapao, O., Thongtem, T., Phuruangrat, A., Thongtem, S., 2013a. Ultrasonic-assisted synthesis of Nd-doped ZnO for photocatalysis. Mater. Lett. 90, 83–86.
Yayapao, O., Thongtem, T., Phuruangrat, A., Thongtem, S., 2013b. Sonochemical synthesis of Dy-doped ZnO nanostructures and their photocatalytic properties. J. Alloys Compd. 576, 72–79.
Yi, S., Cui, J., Li, S., Zhang, L., Wang, D., Lin, Y., 2014. Enhanced visible-light photocatalytic activity of Fe/ZnO for rhodamine B degradation and its photogenerated charge transfer properties. Appl. Surf. Sci. 319, 230–236.
Yu, C., Yang, K., Shu, Q., Yu, J.C., Cao, F., Li, X., 2011. Preparation of WO_3/ZnO composite photocatalyst and its photocatalytic performance. Chin. J. Catal. 32 (3–4), 555–565.
Yu, K.S., Shi, J.Y., Zhang, Z.L., Liang, Y.M., Liu, W., 2013. Synthesis, characterization, and photocatalysis of ZnO and Er-Doped ZnO. J. Nanomater. 2013, 5. Article ID 372951.
Yusoff, N.A., Ong, S.A., Ho, L.N., Wong, Y.S., Khalik, W.F., 2014. Degradation of phenol through solar-photocatalytic treatment by zinc oxide in aqueous solution. Desalin. Water Treat. 54 (6), 1621–1628.
Zhai, J., Tao, X., Pu, Y., Zeng, X.-F., Chen, J.F., 2010. Core/shell structured ZnO/SiO_2 nanoparticles: preparation, characterization and photocatalytic property. Appl. Surf. Sci. 257 (2), 393–397.
Zhai, Y.J., Li, J.H., Fang, X., Chen, X.Y., Fang, F., Chu, X.Y., Wei, Z.P., Wang, X.H., 2014. Preparation of cadmium-doped zinc oxide nanoflowers with enhanced photocatalytic activity. Mater. Sci. Semicond. Process. 26 (1), 225–230.
Zhang, D., Zeng, F., 2012. Visible light-activated cadmium-doped ZnO nanostructured photocatalyst for the treatment of Methylene Blue dye. J. Mater. Sci. 47 (5), 2155–2161.
Zhang, H., Zong, R.L., Zhu, Y.F., 2009a. Photocorrosion inhibition and photoactivity enhancement for zinc oxide via hybridization with monolayer polyaniline. J. Phys. Chem. C 113, 4605–4611.
Zhang, L.W., Cheng, H.Y., Zong, R.L., Zhu, Y.F., 2009b. Photocorrosion suppression of ZnO nanoparticles via hybridization with graphite-like carbon and enhanced photocatalytic activity. J. Phys. Chem. C 113 (11), 2368–2374.
Zhang, Y., Chen, Z., Liu, S., Xu, Y.J., 2013. Size effect induced activity enhancement and anti-photocorrosion of reduced graphene oxide-ZnO composites for degradation of organic dyes and reduction of Cr(VI) in water. Appl. Catal. B Environ. 140–141, 598–607.
Zhang, C., Zhang, J., Su, Y., Xu, M., Yang, Z., Zhang, Y., 2014a. ZnO nanowire/reduced graphene oxide nanocomposites for significantly enhanced photocatalytic degradation of Rhodamine 6G. Phys. E Low Dimens. Syst. Nanostructures 56, 251–255.
Zhang, P., Hong, R.Y., Chen, Q., Feng, W.G., 2014b. On the electrical conductivity and photocatalytic activity of aluminum-doped zinc oxide. Powder Technol. 253, 360–367.
Zhang, X., Qin, J., Xue, Y., Yu, P., Zhang, B., Wang, L., Liu, R., 2014c. Effect of aspect ratio and surface defects on the photocatalytic activity of ZnO nanorods. Sci. Rep. 4, 4596.
Zhang, X., Dong, S., Zhou, X., Yan, L., Chen, G., Dong, S., Zhou, D., 2015. A facile one-pot synthesis of Er-Al co-doped ZnO nanoparticles with enhanced photocatalytic performance under visible light. Mater. Lett. 143, 312–314.
Zhao, Z., Song, J.-L., Zheng, J.-H., Lian, J.-S., 2014. Optical properties and photocatalytic activity of Nd-doped ZnO powders. Trans. Nonferrous Metals Soc. China 24 (5), 1434–1439.
Zheng, Y., Chen, C., Zhan, Y., Lin, X., Zheng, Q., Wei, K., Zhu, J., Zhu, Y., 2007. Luminescence and photocatalytic activity of ZnO nanocrystals: correlation between structure and property. Inorg. Chem. 46 (16), 6675–6682.
Zhong, J.B., Li, J.Z., He, X.Y., Zeng, J., Lu, Y., Hu, W., Lin, K., 2012a. Improved photocatalytic performance of Pd-doped ZnO. Curr. Appl. Phys. 12 (3), 998–1001.
Zhong, J.B., Li, J.Z., Lu, Y., He, X.Y., Zeng, J., Hu, W., Shen, Y.C., 2012b. Fabrication of Bi^{3+}-doped ZnO with enhanced photocatalytic performance. Appl. Surf. Sci. 258 (11), 4929–4933.
Zhou, X., Shi, T., Zhou, H., 2012. Hydrothermal preparation of ZnO-reduced graphene oxide hybrid with high performance in photocatalytic degradation. Appl. Surf. Sci. 258 (17), 6204–6211.
Zong, Y., Li, Z., Wang, X., Ma, J., Men, Y., 2014. Synthesis and high photocatalytic activity of Eu-doped ZnO nanoparticles. Ceram. Int. 40 (7, Part B), 10375–10382.
Zsigmond, P., 2014. Different silver-modified zinc oxides for photocatalytic degradation of imidacloprid. Chemija 25 (1), 1–4.